Key Points:
- The extratropical response of Madden Julian Oscillation in current Reanalysis may not be robust due to limited sample size
- Strongest extratropical response is induced when Madden Julian Oscillation propagates through specific phases, instead of a single phase
- The amplitude, duration, and timing of the extratropical response strongly depend on initiation and decay of Madden Julian Oscillation

Correspondence to:
C. Zheng,
cheng.zheng.1@stonybrook.edu

The Role of MJO Propagation, Lifetime, and Intensity on Modulating the Temporal Evolution of the MJO Extratropical Response

C. Zheng[1] and E. K. M. Chang[1]

[1]School of Marine and Atmospheric Sciences, Stony Brook University, Stony Brook, NY, USA

Abstract The Madden-Julian Oscillation (MJO) is the dominant mode of tropical intraseasonal variability. Many studies have found that the MJO has significant impacts on extratropical weather. Since the MJO can act as a tropical heat source that excites Rossby waves, midlatitude weather is modulated by the MJO due to the Rossby waves that propagate into the midlatitude and modulate the midlatitude circulation. Heat sources of individual MJO events are different since each event has different eastward propagation speed, lifetime, intensity, and structure. The background flow is also different for each event. These result in different Rossby waves and different extratropical response for each MJO event. In this study, the role of MJO propagation speed, lifetime, and intensity on modulating the structure and temporal evolution of the MJO extratropical response is systematically explored by using an idealized general circulation model. By adding the MJO-associated heating into the general circulation model as an external forcing, the extratropical response in the Reanalysis is captured reasonably by the model. However, large ensemble model simulations show that the response in the Reanalysis is not robust. Experiments with MJO events of different propagation speed, lifetime, and intensity show that to excite a strong extratropical response, the MJO has to propagate through specific phases (Phases 1–3 and 5–7). The intensity, timing, and duration of the extratropical response strongly depend on when the MJO is initiated and when the MJO decays. The extratropical impacts of slow- and fast-propagating MJO also have significant differences, especially on intensity and duration.

1. Introduction

The Madden-Julian Oscillation (MJO), the dominant mode of intraseaonal tropical variability, is characterized by large-scale eastward propagating tropical convection (Madden & Julian, 1971, 1972, 1994) from the Indian Ocean through the maritime continent to the western Pacific, accompanied by an associated dynamical and thermodynamical structure. Though the convective features of the MJO are mostly over the warm pool region, the associated circulation has a global scale in the tropics. In addition, the impact of the MJO on circulation is not limited to the tropics. Many studies (e.g., Hoskins & Karoly, 1981; Jin & Hoskins, 1995; Sardeshmukh & Hoskins, 1988) have shown that stationary Rossby waves can be excited by tropical diabatic heating source, which acts as the source of Rossby waves, and the Rossby waves, which propagate into the extratropics, can significantly modulate midlatitude circulation. Thus, the eastward moving convection associated with the MJO can act as the diabatic heating source and modify extratropical circulation (e.g., Matthews et al., 2004; Riddle et al., 2013; Seo & Son, 2012). Previous studies have found that some important modes of climate variability can be modulated by the MJO, including the North Atlantic Oscillation (e.g., Cassou, 2008; Lin et al., 2009), the Arctic Oscillation (e.g., Flatau & Kim, 2013; L'Heureux & Higgins, 2008; Zhou & Miller, 2005), and the Pacific-North American pattern (e.g., Mori & Watanabe, 2008; Schreck et al., 2013).

Midlatitude surface weather, such as surface air temperature, precipitation, and extratropical cyclone activity, can also be modulated by the MJO (e.g., Zheng et al., 2018). The MJO can modulate the surface air temperature at high latitude (Vecchi & Bond, 2004; Yoo et al., 2011), over Canada (Lin & Brunet, 2009) and the United States (Zhou et al., 2012). Anomalous precipitation over North America can also be induced by the MJO (e.g., Baxter et al., 2014; Becker et al., 2011; Donald et al., 2006; Lin et al., 2010; Zhou et al., 2012). Extratropical cyclones, which account for much of the high-impact weather in winter, including extreme cold, high wind, and heavy precipitation events (e.g., Kunkel et al., 2012; Ma & Chang, 2017), are also significantly modulated by the MJO. The MJO modulation on extratropical cyclone activity is not limited to

over the Pacific (Deng & Jiang, 2011; Lee & Lim, 2012) but also extends into North America, North Atlantic, and northern Europe (Grise et al., 2013; Guo et al., 2017).

Zheng et al. (2018) found that the MJO impacts on surface weather can be explained by the circulation anomalies induced by the MJO. The signal-to-noise ratio of the MJO extratropical impact has been quantified, and it shows that the MJO impacts on extratropical cyclone activity are most important over the eastern North Pacific, Canada, southeast United States, and the central North Atlantic, whereas the MJO impacts on surface air temperature are most significant over the eastern U.S. These anomalies are linked to the tropics through Rossby wave trains induced by the MJO. The upper level circulation anomalies associated with the Rossby wave enhance/suppress the zonal wind, which modulates the extratropical cyclone activity. As the circulation anomalies are equivalent barotropic, warm/cold advection will also be induced by the Rossby waves, which give rise to the temperature anomalies. Therefore, the upper level Rossby wave train is very important as it connects the MJO and extratropical surface weather anomalies. Furthermore, the strongest MJO extratropical response is found 1 or 2 weeks after specific MJO phases instead of happening simultaneously when the MJO has large amplitude. Given that the MJO can be predicted out to 3 to 4 weeks (e.g., Kim et al., 2014; Lim et al., 2018; Vitart, 2017; Xiang et al., 2015), the MJO-forced signal can be very useful for subseasonal predictions (e.g., Tseng et al., 2018). Note that many studies used the Real-time multivariate MJO (RMM) index (Wheeler & Hendon, 2004), which includes both MJO-associated convection and circulation, to evaluate the MJO prediction skill in dynamical models. Several studies have suggested that the MJO-associated circulation is more predictable than MJO-associated convection (e.g., Kim et al., 2014; Klingaman et al., 2015).

Multiple factors can modulate the MJO extratropical response. As the background flow in the extratropics determines how Rossby waves propagate and evolve, the MJO extratropical response will be different if the background flow changes (e.g., Goss & Feldstein, 2015; Henderson et al., 2017). Each MJO event can have different initiation/decaying location, propagation speed, and lifetime, and as both enhanced and suppressed convection can act as diabatic heating source to induce Rossby waves (Seo & Lee, 2017), the Rossby wave source can be different for individual MJO event. Thus, the Rossby wave trains for each MJO event can be very different. For example, slow-propagating MJO events are found to have much stronger response over North Atlantic than fast-propagating events (Yadav & Straus, 2017). This is important for subseasonal prediction, since the prediction is more related to what extratropical signal will be induced by the current, specific MJO event, rather than what the mean MJO extratropical response (averaged over multiple MJO events) is. However, in most of the previous studies, only the mean MJO extratropical response has been investigated. In addition, only since the satellite era (after 1979) has there been extensive observational coverage over the extratropical oceans. While the RMM index can be reconstructed back to 1905 based on tropical circulation information alone (Oliver & Thompson, 2012), it is not clear whether one can confidently reconstruct the MJO-related extratropical circulations prior to the satellite era. Thus, the number of MJO events that can be used to reconstruct the MJO extratropical response is limited, and it is possible that even in terms of the mean MJO extratropical response, the signal from the Reanalysis data may not be robust (see section 3). Furthermore, non-MJO-related variabilities in the extratropics can give rise to noise of large amplitudes when analyzing the MJO extratropical impact. This makes it hard to separate the differences of the extratropical response induced by individual MJO events in the Reanalysis data. Thus, modeling study is necessary to examine the differences in the extratropical responses related to differences in MJO forcing. An idealized general circulation model (GCM) will be used in this study. Large ensembles can be performed using this idealized GCM, as it can be run at a low computational cost. We will see that this is beneficial in separating the MJO signal from the noise to get statistically significant results.

In section 2, the data and the idealized GCM will be introduced. How we put the MJO heating into the model and how different sets of experiments are designed will be discussed. In section 3, the MJO extratropical response in the model will be compared with the Reanalysis data to examine whether the model generates reasonable results. The response to MJO events with different lifetimes, propagation speed, initiation/decaying phase, and intensity will be investigated in section 4. Results from a stationary wave model will be briefly discussed in section 5. Some implications for subseasonal forecast and the conclusions will be presented in section 6.

2. Data and Idealized GCM

2.1. Data

The RMM index, a commonly used MJO index, is applied to define the MJO in this study. The RMM index is developed based on multivariate empirical orthogonal function analysis of the combined fields of outgoing longwave radiation (OLR), 850- and 200-hPa zonal wind anomalies. The first two leading normalized principal components are referred to as RMM1 and RMM2. Based on the sign and amplitude of RMM1 and RMM2, the MJO eight-phase life cycle can be defined. The location of enhanced and suppressed convection associated with different RMM phases has been shown in Wheeler and Hendon (2004) by compositing OLR anomalies. The days when the amplitude of RMM index is greater than 1 ($\sqrt{\mathrm{RMM1}^2 + \mathrm{RMM2}^2} \geq 1$) are defined as the *strong* MJO days in this study. We also performed some experiments by applying heating using an OLR-based MJO index (OMI; Kiladis et al., 2014), and the results are very similar.

This study uses European Centre for Medium-Range Weather Forecasts Interim Re-Analysis (ERA-Interim; Dee et al., 2011) 6-hourly geopotential height at 300 hPa on a 2.5° by 2.5° horizontal resolution grid to quantify the MJO extratropical response. The upper level height anomalies will be the focus of this study, as it highlights the Rossby wave train (see section 3.1), and the Rossby wave train connects the MJO and the extratropics. Following Zheng et al. (2018), data in extended boreal winter (November–April) from 1979 to 2016 are used in this study. After converting the temporal resolution from 6-hourly to daily, daily climatology is removed prior to making the MJO composites from Reanalysis data. The composite of MJO extratropical response is made by using all the days when RMM index amplitude is larger than 1 in the extended boreal winter (November–April). Temperature tendency from diabatic processes, a forecast product from ERA-Interim, which represents diabatic heating, is initialized at 00 and 12 UTC each day and outputs over ranges of 3, 6, 9, and 12 hr at 60 model levels and on a 0.75° by 0.75° horizontal resolution grid. We use the temperature tendency from diabatic processes to construct the MJO-related diabatic heating in the idealized GCM (see section 2.3). OLR, which is usually used to illustrate the convection in the tropics, is obtained from NOAA Interpolated Outgoing Longwave Radiation data set (Liebmann & Smith, 1996).

2.2. Idealized GCM

A dry idealized GCM, which has the same configuration as Xia and Chang (2014), has been used to study the MJO extratropical response. This model has been introduced by Chang (2006, 2009). The model is based on the dynamical core of the Geophysical Fluid Dynamics Laboratory global spectral model (Held & Suarez, 1994). We run the model with 20 evenly distributed sigma levels in the vertical and horizontal resolution of T42 (~2.8° resolution). Realistic orography smoothed to model resolution is imposed. A land-sea mask is used with stronger friction over land. The only other forcing imposed, apart from the orography, is Newtonian cooling to a radiative equilibrium temperature profile, together with scale-selective diffusion. The first law thermodynamics can be written as

$$\frac{D\theta}{Dt} = -\frac{\theta - \theta_E}{\tau} - \kappa \nabla^8 \theta \tag{1}$$

where τ is the radiative timescale and θ_E can be split into two parts:

$$\theta_E = \theta_C - \tau Q \tag{2}$$

Here θ_C can be considered as the desired model climatology and Q to be the diabatic heating distribution, which is initially unknown. As described in Chang (2006), with an iteration process for the heating profile (Q) to force the model, at the end of the process, the model climate, as given by the time mean three-dimensional temperature distribution (here we use National Centers for Environmental Prediction-National Center for Atmospheric Research [NCEP-NCAR] reanalysis to define this climate), is nearly identical to the desired target temperature distribution θ_C. To enhance the amplitude of the eddies to be close to that in the reanalysis data set, the static stability is reduced in the target climate temperature profile to mimic the impact of moist effects in amplifying eddy amplitudes in this dry model (see also O'Gorman, 2011).

$$\theta_C = \theta_{\mathrm{obs}}(x, y, p) - A z(p) \tag{3}$$

where θ_{obs} is climatological January potential temperature distribution taken from NCEP-NCAR reanalysis. Following Chang (2009) and Xia and Chang (2014), $A = 0.65$ K/km. More details concerning the model formulation and the iterative process can be found in Chang (2006). Note that transients of all timescales are present in the idealized GCM simulations, and Chang (2006, 2009) demonstrated that the model can reproduce the observed midlatitude climate, including the storm tracks, reasonably well.

Moist processes in the extratropics may influence the MJO-induced Rossby wave train. Heavy precipitation may favor regions at the leading edge of the troughs, which can be associated with the MJO-induced wave train. Blocking events are also associated with MJO (e.g., Henderson et al., 2016, Moore et al., 2010), and blocking can be amplified by moist processes (e.g., Pfahl et al., 2015). Though the static stability is reduced in the model to mimic the impact of moist effects, these processes are not explicitly simulated by the model. In addition, with limited vertical levels, stratosphere is not well resolved in the model. The interaction between MJO and stratospheric anomalies (e.g., Garfinkel et al., 2012) may not be well simulated by this model.

2.3. MJO-Related Heating as the External Forcing of the Idealized GCM

The MJO-related heating does not exist in our simple idealized GCM since latent heating is not explicitly simulated. To simulate the MJO extratropical response, the MJO-related diabatic heating is added into the model as an external forcing. The MJO-related diabatic heating is obtained with the following steps: (1) Temperature tendency from diabatic processes data from ERA-Interim is horizontally interpolated onto a 2.5° by 2.5° resolution grid and then vertically interpolated from ERA-Interim model levels to the sigma levels in the idealized GCM. (2) The 12-hourly temperature tendency data are converted to daily data. (3) Following the procedure of generating the RMM index, the time mean and first three spherical harmonics of the annual cycle is removed at each grid point. Then a 120-day mean of previous 120 days is subtracted at each grid point to remove any further aspects of interannual variability, decadal variability, and trends. (4) Consider that there is significant seasonality in the MJO (e.g., Zhang & Dong, 2004), and we are just focusing on boreal winter; the RMM1- and RMM2-associated heating Q_{RMM1} and Q_{RMM2} are represented as the regression of temperature tendency anomaly data onto December to February RMM1 and RMM2 indices, respectively. (5) Q_{RMM1} and Q_{RMM2} are horizontally interpolated onto the model grid (T42, shown in Figure S1 in the supporting information). (6) Q_{RMM1} and Q_{RMM2} are set to zero at grid points north of 15°N or south of 20°S to eliminate any extratropical diabatic heating, which is not directly associated with the MJO tropical convection. (7) For any given RMM phase and amplitude, if we know rmm1 = RMM1 and rmm2 = RMM2 (RMM1 and RMM2 represent the observed RMM indices, while rmm1 and rmm2 can represent any observed or idealized evolution of the RMM indices), the MJO-related heating Q_{MJO} can be constructed with the equation:

$$Q_{\mathrm{MJO}} = \mathrm{rmm1} \times Q_{\mathrm{RMM1}} + \mathrm{rmm2} \times Q_{\mathrm{RMM2}} \tag{4}$$

Then Q_{MJO} can be imposed into the idealized model as the diabatic heating associated with the MJO. Different sets of experiments have been performed with different Q_{MJO} (see Table 1). Details of these experiments are discussed in sections 3 and 4. Similar to the Reanalysis, the 300-hPa height from the model is used to investigate the MJO extratropical response.

The OMI index, which is just based on OLR, has also been used to construct the heating, and the results from those experiments are similar to those presented below. This gives us confidence to use the RMM index to both construct heating pattern and identify extratropic response in the model, though RMM index is dominated by circulation instead of convection (e.g., Straub, 2013). For individual MJO events, the spatial structure of the convection can vary a lot even if the RMM (or OMI) index is in the same phase. The spatial pattern of heating in the tropics is important to the extratropical response (e.g., Goss & Feldstein, 2017). This spatial variability of the MJO heating is not captured by constructing the MJO heating by regression onto the RMM index. However, as this study focuses on testing how initiation, decay, and propagation of MJO modify extratropical response, fixed spatial patterns of MJO heating related to RMM1 and RMM2 are required in modeling experiments. The heating structure based on regression, which represents the on-average MJO heating,

Table 1
Description of Model Experiments in this Study

Experiments	Description	Ensemble size	Experiments duration
REAL_MJO	Use *realistic* MJO heating as external forcing	1,000	37 winter seasons (October to April in 1979–2016)
NON_PROP	Use realistic MJO heating as external forcing, but the MJO heating is modified to make it not eastward propagating	1,000	37 winter seasons (October to April in 1979–2016)
FAST_MJO	Use realistic MJO heating as external forcing, but the MJO is propagating 2 times faster	1,000	37 winter seasons (October to April in 1979–2016)
SLOW_MJO	Use realistic MJO heating as external forcing, but the MJO is propagating 2 times slower	1,000	37 winter seasons (October to April in 1979–2016)
PHASE_s->e	Idealized MJO heating with MJO starts at phase s and ends at phase e, both s and e can be any phase from phase 1 to 8. The propagation speed is 5 or 8 days per phase.	1,000	60 days if the propagation speed is 5 days per phase, 80 days if the propagation speed is 8 days per phase
PHASE(m)_(n) days	Stationary phase m MJO heating lasts for n days. Phase m can be any phase from Phases 1 to 8. Heating duration n can be 5, 10, 15, or 20 days.	1,000	60 days for each run
CYCLIC_MJO	Continuous MJO heating from Phases 1 to 8 and back to 1 for 12 cycles. MJO propagates at a speed of 5 days per phase	1,000	480 days for each run

is a reasonable heating pattern to be used. The conclusions in the following parts of the study that different MJO lifecycle could give rise to different evolution of midlatitude response will not be changed if we consider the impact of differences in the heating structure across different MJO events.

Extratropical circulation also influences the initiation, strengthening, and propagation of the MJO (e.g., Adames et al., 2014; MacRitchie & Roundy, 2016; Ray et al., 2009; Ray & Li, 2013; Zhao et al., 2013) and MJO prediction (e.g., Lin & Brunet, 2011; Vitart & Jung, 2010). However, as the MJO heating is prescribed in our dry GCM, only the MJO influence on the extratropics is tested. The extratropical impact on MJO is excluded with our experiment setup.

2.4. Stationary Wave Model

Stationary wave model experiments have been shown by previous studies (e.g., Held et al., 2002; Wang & Ting, 1999) to be a powerful diagnostic tool for understanding the maintenance of stationary planetary waves. As the MJO-excited Rossby waves are quasi-stationary (e.g., Zheng et al., 2018), the stationary wave model can also be useful to analyze the MJO extratropical response. The stationary wave model used in this study is modified from the idealized GCM such that synoptic-scale transients are absent, and only the low-frequency response to tropical heating is simulated. The approach is very similar to Yang and Chang (2006). Details about the model can be found in Text S1. Experiments parallel to those in the idealized GCM have been conducted using the stationary wave model to provide an additional scope to analyze the MJO extratropical response.

3. Realistic MJO Heating

3.1. Reanalysis

As shown by previous studies (e.g., Baxter et al., 2014; Lin & Brunet, 2009; Zheng et al., 2018), lag composites of upper level stream function anomalies or geopotential height anomalies can be useful to depict the Rossby Wave train excited by the MJO. The lag composites of 300-hPa geopotential height anomaly of RMM Phase 3 (one of the phases that MJO extratropical response is strongest based on previous studies) in ERA-Interim data are shown in Figures 1a–1e. At lag day 0, positive height anomaly is associated with the enhanced convection over the Indian Ocean, while negative anomaly is associated with suppressed convection over western Pacific, which is shown by the OLR anomalies. A positive height anomaly has developed over central North Pacific, and a negative height anomaly is over Alaska and western Canada. This clearly shows the pattern of the Rossby wave. As the Rossby wave train propagates, positive anomaly develops over eastern North America, and the anomalies over central North Pacific and Alaska are enhanced. The positive anomaly over eastern North America can last more than 15 days and has significant impact on weather over the nearby regions (Zheng et al., 2018).
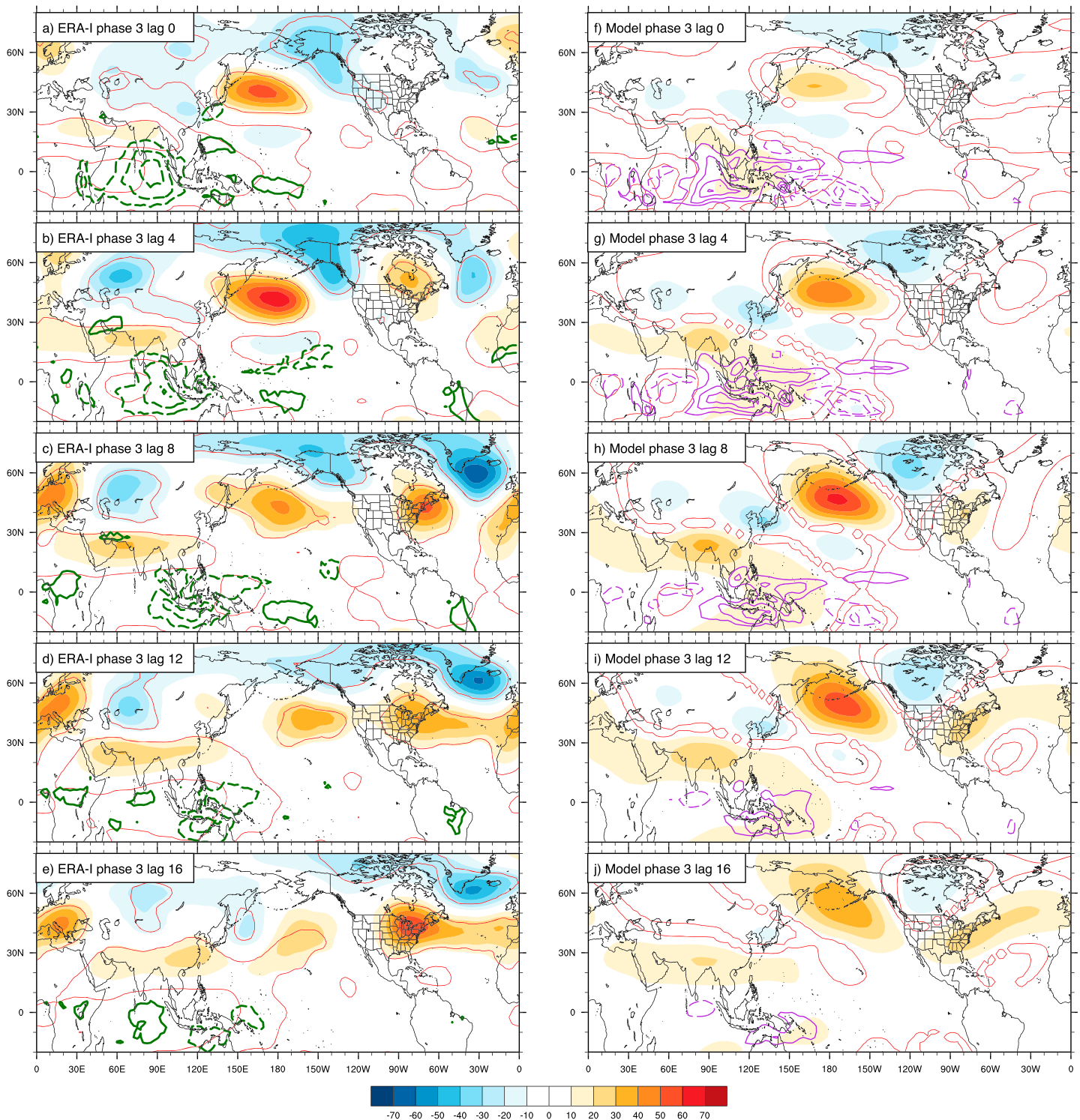
Figure 1. (a–e) RMM Phase 3 lag composites of 300-hPa geopotential height anomaly based on ERA-Interim Reanalysis (units in m). The red contours outline the regions where the height anomaly is statistically significant at the 95% level from the results of a Monte Carlo test (following the methods in Zheng et al., 2018). The dark green contours show the OLR anomalies. Solid contours are positive, dashed contours are negative, and the zero contour is omitted. Contour interval is 8 W/m² . (f–j) The same as (a)–(e), but for 300-hPa geopotential height anomaly in idealized model experiments (REAL_MJO). The violet contours show the mean temperature tendency from surface to 100 hPa in the model. The temperature tendency is an external forcing added into the model to mimic the MJO heating. Solid contours are positive, dashed contours are negative, and the zero contour is omitted. Contour interval is 0.25 K/day. Note that as the ensemble size is large, most of the anomaly from REAL_MJO experiments are statistically significant (as shown by the red contour).
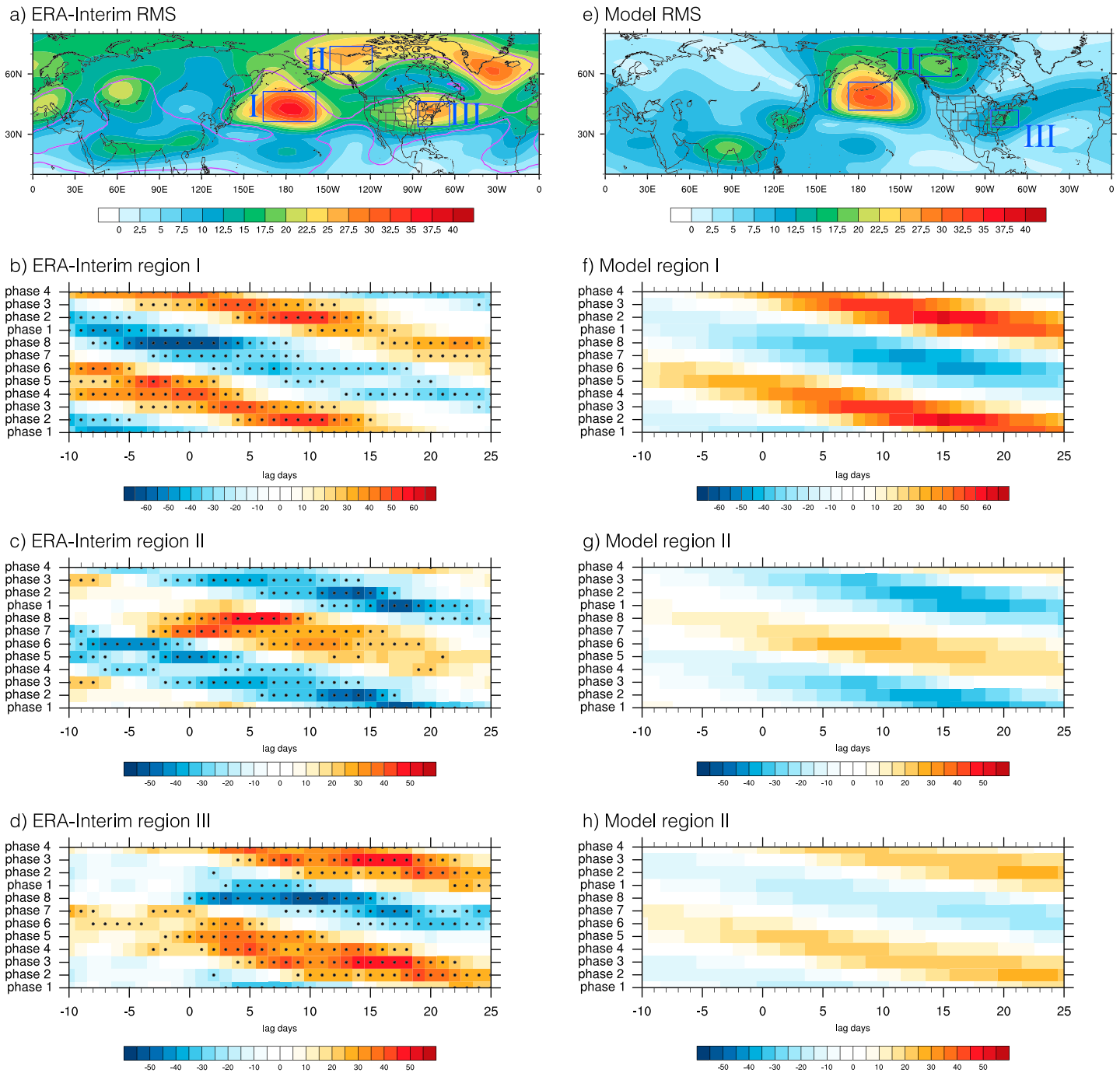
Figure 2. (a) Root-mean-square (RMS) of the 300-hPa geopotential height anomaly (similar to Figure 1a) of eight RMM phase and lag days from 0 to 25 (units in m). The purple line depicts the regions where the RMS exceeds 95% statistical significance level in a Monte Carlo test. (b–d) Lag composites of 300-hPa geopotential height of eight RMM phases and lag days from −10 to 25 for Regions I, II, and III, respectively. The locations of the three regions are shown in (a). Dotted days are statistically significant at the 95% level from the results of a Monte Carlo test (following Zheng et al., 2018). (e−h) The same as (a)−(d) but for REAL_MJO experiments. Note that the statistical significance levels are not shown in (f)−(h). As the ensemble size in REAL_MJO is large, all the nonwhite shading in (f)−(h) are statistically significant.

Similar lag composites of the eight RMM phases and lag days from 0 to 25 have been made (a total of 208 lag composites). To better summarize the MJO impacts on geopotential height from these composite maps, the root-mean-square (RMS) of the anomalies at each grid point in these maps has been plotted in Figure 2a. Grid points where the MJO can induce large positive or negative height anomalies will show large values

in the RMS map; MJO impact is small if the RMS is small over an extratropical grid point. The RMS map highlights three regions that have been discussed above: central North Pacific, Alaska and western Canada, and eastern North America (the region with high RMS near Greenland will not be the focus in this study; see Text S2). We name the three regions as Regions I, II, and III, respectively, and calculate the area-averaged height anomalies over the three regions (Figures 2b–2d). In each region, similar signal after any phase can generally be found at roughly 5 days earlier than after the following RMM phase (e.g., positive signal after Phase 3 in Region I is earlier than that after Phase 2), which is consistent with the propagation of the MJO (as shown in Wheeler & Hendon, 2004, the correlation between RMM1 and RMM2 maximizes at a 9-day lag, which means that the RMM index propagates at a speed of 4–5 days per phase). Comparison among the three regions shows that the positive signal in Region II appears after the negative signal in Region I in the same phase (e.g., negative signal in Region II Phase 2 is a few days later than the positive signal in Region I Phase 2) and appears earlier than the negative signal in Region III in the same phase (e.g., negative signal in Region II Phase 2 is a few days earlier than the positive signal in Region III Phase 3). Similar behaviors can also be seen for the opposite phases. This shows how the Rossby wave train propagates. As the wave train reaches Region I, and then Regions II and III (Figures 1a–1e), the signal in Region I leads that in Region II, and the signal in Region II leads that in Region III. Therefore, the three regions show where the MJO has large impact over North Pacific and North America, and the timing of the signal depicts the propagation of the Rossby wave. In the following parts of this study, we will mainly discuss these three regions. Note that the signal is not sensitive to the location of the boxes. The signal does not change qualitatively if the region is a few grid boxes larger or smaller or the region is moved a few degrees to any direction. As shown in previous studies (e.g., Zheng et al., 2018), the height anomalies in Region I can modulate precipitation over California, anomalies in Region II can impact precipitation over the Pacific northwest, and anomalies in Region III can affect temperature over eastern U.S., and extratropical cyclone activity and precipitation over Canada and southeastern U.S.

3.2. Response to Realistic MJO Heating in the Idealized GCM

Realistic MJO heating has been added into the idealized GCM to see whether the model can capture the MJO extratropical response. To make sure that the results from the model are statistically significant, we run the model with 1,000 ensemble members (see below). To generate the initial condition for the ensemble members, we run the model for 30,000 days without Q_{MJO}. Then all the model states from day 30 on at 30-day intervals are taken as the initial conditions of the ensemble members. After that, we run the model ensembles with Q_{MJO} added in for 37 winter seasons (1979–2016). Q_{MJO} is constructed with equation (4) from the *observational* RMM index. As we are investigating extended boreal winter (November to April), to be consistent, the model extratropical responses are investigated only if Q_{MJO} is constructed from a day between November and April. For all winter seasons, to spin up the model, Q_{MJO} from October is first added in before Q_{MJO} goes through November to April; then the days when Q_{MJO} are from October are excluded while making the MJO lag composites. Here each ensemble member will have the same sample size of MJO events as the Reanalysis. We call this experiment as REAL_MJO in the following discussions.

Lag composites after RMM Phase 3 from the REAL_MJO runs are shown in Figures 1f–1j. The height anomaly over central Pacific and Alaska becomes stronger from lag day 0 to lag day 8, and the height anomaly over eastern North America emerges at lag day 12; the propagation of the Rossby wave train excited by the MJO can be captured by the idealized GCM, though the signal is a few days delayed compared to ERA-Interim and the amplitude of the anomaly is smaller over Alaska and eastern North America. Nevertheless, these anomalies are highly significant due to the large ensemble size. The violet contours, which show the vertically averaged Q_{MJO}, resemble the observational OLR anomalies well. This gives us confidence to use Q_{MJO} to represent MJO heating in the idealized GCM.

Similar RMS plot to Figure 2a is shown in Figure 2e. The model is able to capture the three regions where the MJO induces large upper level geopotential height anomalies. However, the large RMS center is shifted to the north over central Pacific and shifted to the east over western Canada. One possibility is that while the model climatology is the same as the January temperature distribution from NCEP-NCAR reanalysis, the composites from the reanalysis are obtained from November to April; hence, the zonal wind distribution is different for the reanalysis and model. As pointed out by Henderson et al. (2017), the locations where strong MJO extratropical responses differ when the zonal wind patterns change. In this study, we focus

on how the properties of the MJO itself modulate the extratropical response rather than the impacts of different background flow patterns, which will be the focus of a follow up study.

3.3. Robustness of MJO Extratropical Response

The lag composite for Regions I, II, and III for REAL_MJO runs (Figures 2f–2h) is very smooth and continuous, with nice *slope* structure. As we have a large ensemble, all the days with nonwhite color are statistically significant at 95%. Compared to Reanalysis, though much of the signal from the Reanalysis is statistically significant, the signal from the Reanalysis is much noisier (Figures 2b–2d). If the MJO extratropical response signal is robust enough, we expect it to be smoother and more continuous like the REAL_MJO experiments (Figures 2f–2h) instead of what is found in the Reanalysis data. This is not surprising since the sample size of the REAL_MJO experiments is 1,000 times larger than that of the Reanalysis. Though the idealized GCM is much more simplified than real atmosphere and may have longer timescale in low-frequency variability (e.g., Xia & Chang, 2014), one can still use the idealized GCM to roughly estimate how large a sample size is needed to generate a robust signal. In Figures 3a–3d, the results from the first ensemble member of REAL_MJO experiments are shown. The RMS (Figure 3a) is much larger than that in the ensemble mean. Note that this is not because of that some ensemble members have larger RMS of anomalies than the ensemble mean and others have smaller RMS of the anomalies than the ensemble mean. Basically, all individual ensemble members have larger RMS than the ensemble mean (ensemble numbers 2 to 20 are shown in Figures S2 and S3). The reasons are as follows: (1) For each ensemble member, the noise generated by the non-MJO-related phenomena can be superposed onto the MJO signal, while in the ensemble mean, especially in a large ensemble, the noise is averaged out. (2) The MJO extratropical response itself may have substantial internal variability due to modulation by the low-frequency variability in the model atmosphere; therefore, individual member may have its own MJO extratropical response pattern with the strongest signal in slightly different geographic locations. Then the ensemble mean signal will be weaker than individual members. Therefore, it is reasonable that the Reanalysis RMS (Figure 2a) is stronger than that from model ensemble mean (Figure 2e), as the sample size is much larger in Figure 2e. The signal of the individual member is noisy (Figures 3b–3d), but when we average over the first 10 ensemble members (Figures 3e–3h), the signal is much smoother and more continuous. Compared to 1,000-ensemble member mean (Figure 2e), the 10-ensemble member mean signal seems to be robust. The RMS value of lag composite over Region I decreases when the lag composites are made from 1 member to 10 members but does not further decrease when the averaging is over more than 10 members (see Figure S29). This suggests that a sample of 10 times the sizes of the Reanalysis is required for a robust signal. Therefore, considering that the signal is not robust for individual ensemble member (which has the same sample size as the Reanalysis), and robust signal should be smooth and continuous (Figures 2f–2h), which is not the case for Reanalysis (Figures 2b–2d), the signal in current Reanalysis is probably still not robust. Results shown in Figures 2 and 3 suggest that the real MJO midlatitude signal may be weaker than that estimated from the available reanalysis data. Note that even if we apply a 20–100 days band-pass filter on Reanalysis (Figure S4) to highlight the MJO-related signal, the composite still appears noisy and does not seem to be robust.

3.4. Importance of MJO Propagation and Lifetime

Is the eastward propagation and lifetime of MJO important to the MJO extratropical response? Three sets of experiments similar to REAL_MJO with 1,000 ensemble members have been conducted to answer the question. We make the MJO nonpropagating for the first set of experiments (named as NON_PROP). The continuous days of RMM index with amplitude larger than 1 are defined as MJO events. For each MJO event, in all days of this event, RMM1 and RMM2 are replaced as the RMM1 and RMM2 of the day at the middle of the event (e.g., if an MJO event last 30 days, RMM index in day number 15 of the event is used). In this way, the MJO becomes nonpropagating, but the lifetime of the MJO remains the same. Figure 4a shows that in terms of location, whether the MJO is propagating or not does not influence where it generates large upper level height anomalies (Figure 4a), though not all RMM phases will lead to strong height anomalies (Figures 4b–4d). The slope structure almost disappears in these lag composites, which means that these slope structures are definitely related to the propagation of the MJO.

In the FAST_MJO experiment, we simply make the MJO propagates 2 times faster (only use days 1, 3, 5 ... of RMM index to construct Q_{MJO}); in SLOW_MJO experiment, the MJO is propagating at one half of the normal speed (in the RMM index, for each two consecutive days, another day is inserted in between these two
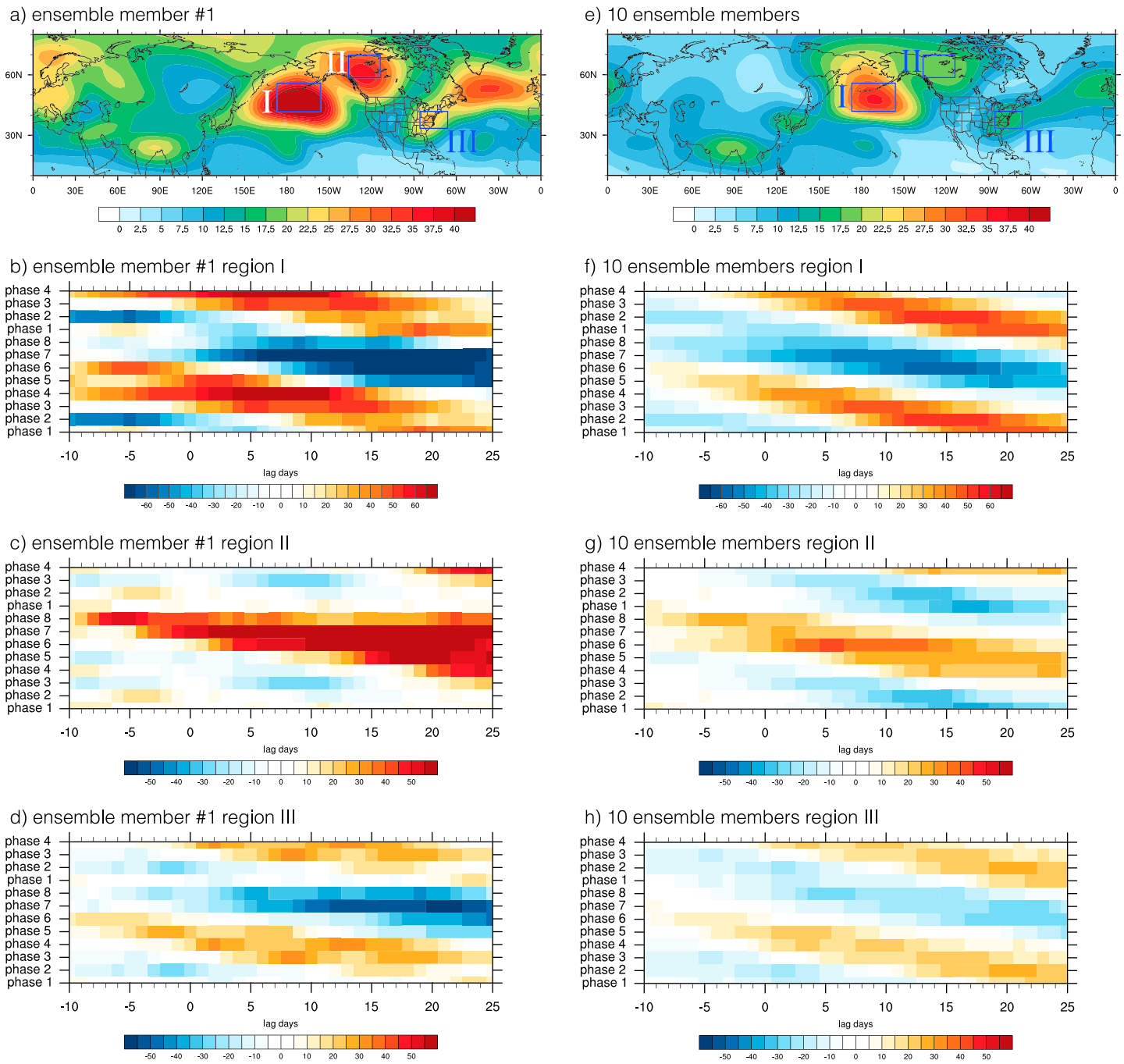
Figure 3. (a−d) The same as Figures 2e−2h, but only use the first ensemble member in REAL_MJO experiments to make the plots. (e−h) The same as Figures 2e−2h, but only use the first 10 ensemble members in REAL_MJO experiments to make the plots.

days with RMM1 and RMM2 equal to the average of RMM1 and RMM2 of these two days, respectively, then Q_{MJO} is constructed with the *new* RMM index). Note that in FAST_MJO and SLOW_MJO, not only the MJO propagation speed is modified, the lifetime is also twice of REAL_MJO in SLOW_MJO experiments and half of REAL_MJO in FAST MJO experiments. The FAST_MJO on average shows much weaker RMS (Figure 4e) compared to when MJO is propagating at a normal speed (Figure 2e), and the SLOW_MJO shows much stronger RMS (Figure 4i). In the lag composites of FAST_MJO and SLOW_MJO (Figures 4g, 4f, 4h, 4j, 4k, and 4l), the slope structure is much steeper in FAST_MJO and is flatter in the SLOW_MJO than that in REAL_MJO (Figures 2f−2h). The amplitude of the MJO extratropical response in FAST_MJO is smaller
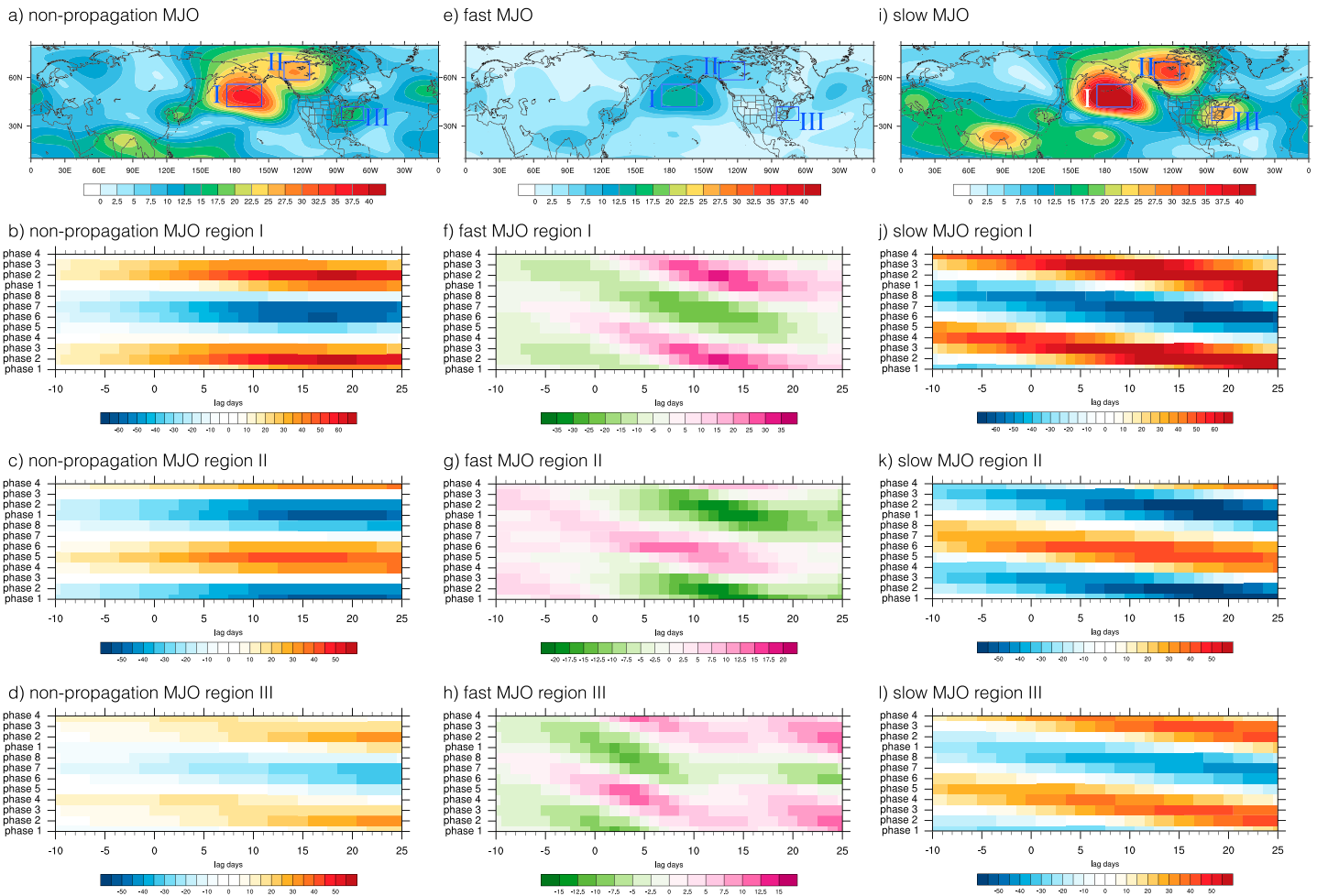
Figure 4. (a−d) The same as Figures 2e−2h, but for NON_PROP experiments. (e−h) The same as Figures 2e−2h, but for FAST_MJO experiments. (i−l) The same as Figures 2e−2h, but for SLOW_MJO experiments.

than that in REAL_MJO, and the amplitude is larger in SLOW_MJO than that in REAL_MJO. This is consistent with Yadav and Straus (2017) that slow-propagating MJO will give rise to stronger extratropical response. The duration of the signal is much longer in the SLOW_MJO cases. The timing is also quite different in the two sets of experiments; for example, for SLOW_MJO, the strongest positive signal in Region III after Phase 3 is from day 13 to day 20, while the counter part for FAST_MJO is separated into two periods, one between day 5 and day 10 and the other is after day 20. Therefore, the propagation speed and lifetime of the MJO modulate the timing, duration, and amplitude of the MJO extratropical response. However, as the number of MJO events is limited in the RMM index, to further study how MJO propagation and lifetime influence the MJO extratropical response, experiments using idealized MJO events (Q_{MJO}) are necessary. This will be discussed in the following section.

4. Idealized MJO Heating

4.1. Idealized MJO Heating Setup

Idealized MJO events have been added into our idealized GCM. Before determining the properties of the idealized MJO events, we first investigate the properties of MJO events in the observed RMM index (Figure 5). The RMM index can sometimes be noisy as non-MJO phenomena can project onto the empirical orthogonal functions of RMM. So we also perform a 5-day running mean on the amplitude of RMM index. The properties of *running mean* RMM index are shown in Figure S28. As mentioned above, we define MJO events as continuous days when RMM index amplitude is greater than 1. Then the number of continuous
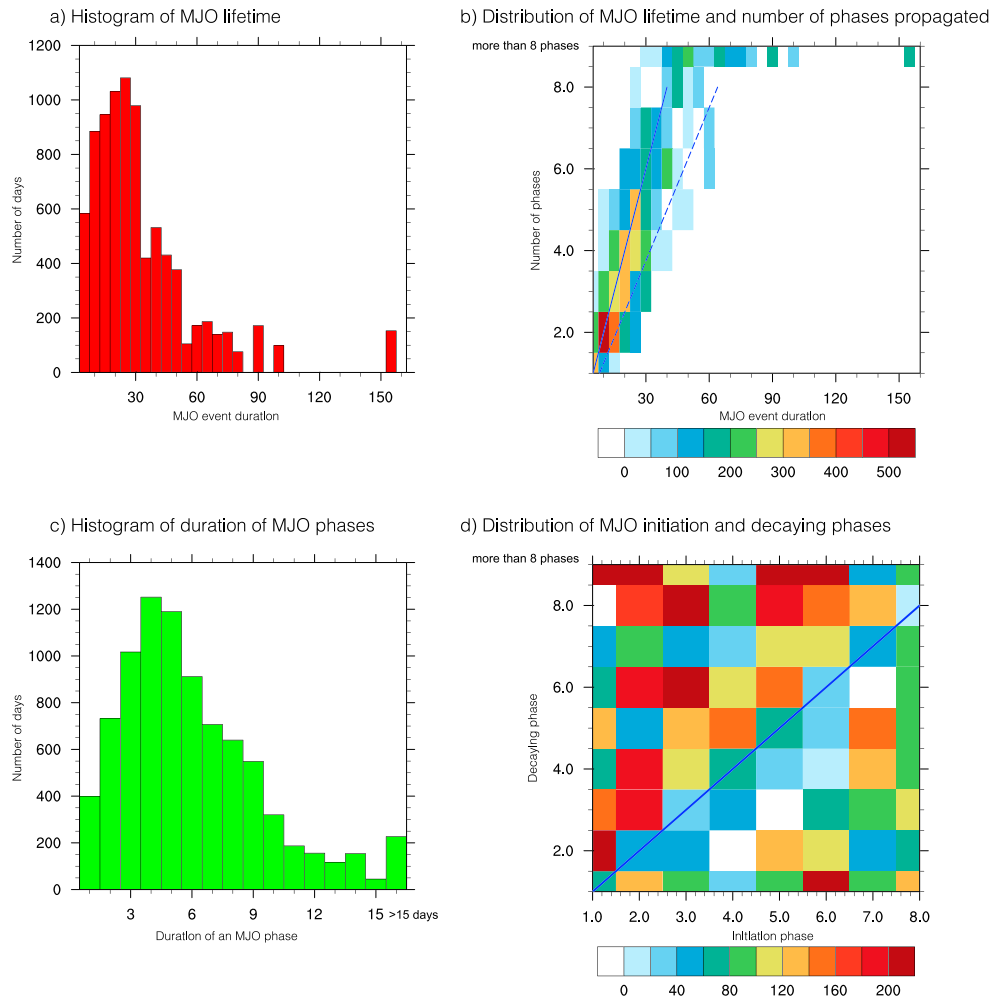
Figure 5. (a) Histogram of MJO lifetime in RMM index from 1979 to 2016. *X* axis is the length of the lifetime, and *Y* axis is the number of days that RMM index amplitude is larger than 1. (b) Distribution of MJO lifetime and number of phases the MJO events propagate. The *X* axis is the length of the MJO lifetime, and *Y* axis is the number of phases the MJO events propagate. The shadings show the number of days that RMM index amplitude is larger than 1. The blue solid line and blue dash line show the MJO propagation speed of 5 and 8 days per phase, respectively. (c) Distribution of duration of RMM phases. The *X* axis is the duration of a single RMM phase, and *Y* axis is the number of days that the MJO propagates through a phase with the duration in *X* axis. (d) Distribution of MJO initiation and decaying phases. The *X* axis is the initiation phase of the MJO, and the *Y* axis is the decaying phase of the MJO. If the MJO propagates a complete MJO life cycle (e.g., starting from Phase 1 and propagating to Phase 8 and then to Phase 1), it is shown in the top row. The shadings show the number of MJO days of each initiation and decaying phase.

days is the lifetime of MJO event. In Figures 5a and S28a, in most of the days when RMM index amplitude is greater than 1, the MJO lifetime is shorter than 50 or 60 days. Figures 5b and S28b show that more than half of the days when MJO is strong, the MJO events propagate less than one life cycle (eight phases). The propagation speed of the MJO can be defined as how many days MJO can propagate from one phase into the following phase (units in days per phase). The average propagation speed of RMM index is 4–5 days per phase (see section 3.1). The solid blue line in Figure 5b, which represents that the MJO is propagating at a speed of 5 days per phase, picks up the majority of the strong MJO days. A few events propagated faster than 5 days per phase; however, as shown in section 3.4 that fast-propagating MJO events on average do not induce strong extratropical response, these fast-propagating events will not be our focus. There are quite a few events that propagate slower than 5 days per phase, but most of them propagate faster or near 8 days per phase (dash blue line in Figure 5b). The distribution of duration of each phase (Figure 5c) shows that the duration peaks at 4 or 5 days, and in much fewer days the duration of an RMM phase is longer than 9 days, which is consistent with the lag-correlation analysis of Wheeler and Hendon

(2004; see section 3.1). The peak of the RMM index spectrum is between 30 and 80 days (see Wheeler & Hendon, 2004), which is also the major time frequency of MJO. The distribution of duration of each phase peaks at 5 or 6 days if we filter the RMM data by a 30–80-day band-pass filter (not shown). One possible reason is that some high-frequency phenomena like Kelvin waves project onto RMM index pattern and skew the duration of average MJO propagation speed. Though the peak of the duration is different by using different method, the peak is near 5 days per phase. This mean that it is reasonable to use 5 days per phase to represent the average MJO propagation speed. Therefore, in our idealized MJO events, the MJO will be propagating either at 5 days per phase or at 8 days per phase. Note that raw RMM index is dominated by short events that propagate less than three phases (Figure 5b). This is not the case in the running mean RMM index (Figure S28b), which suggests that substantial number of the short events in the raw RMM index can be regarded as parts of longer events.

As shown in Straub (2013) and Matthews (2008), though the Indian Ocean is the favorable location for MJO to be initiated, the MJO actually can be initiated at any phase. Therefore, our idealized MJO events will start at all eight RMM phases. The duration of the MJO events is set from one phase to eight phases, as shown in Figure 5b that in few cases the MJO can be strong for a complete cycle. A total of 64 sets of experiments (8×8 different MJO heating) have been performed. For each set of experiments, if we use s (start) to represent the initiation phase and e (end) to represent the ending phase of the MJO event, then this set of experiments can be represented as PHASE_s->e. Most of the 64 types of MJOs have been observed. As shown in Figure 5d, only four cases of the 64, PHASE_1->8, PHASE_4->2, PHASE_5->3, and PHASE_7->6, have not been observed. Thus, it is useful to analyze all the 64 sets of experiment. Note that in our idealized MJO events, lifetime (days) equals to propagation speed (days per phase) multiplied by the number of phases MJO propagates through. Therefore, lifetime, propagation speed, and number of phases MJO propagates are not independent. Since the propagation speed is set to either 5 or 8 days per phase, we can focus on modifying the number of phases MJO propagates through instead of directly modifying MJO lifetime.

One interesting question is if the heating does not propagate, which RMM phases can excite the strongest extratropical response? Experiments with stationary Q_{MJO} (the MJO stays in one specific RMM phase and does not propagate) have been done. The duration of the heating in these experiments is 5, 10, 15, or 20 days long. If the heating is in phase m and lasts n days, the set of experiments is called PHASE(m)_(n)days (Table 1). To further study the impact of MJO propagation, we also have a set of experiments called CYCLIC_MJO, in which the MJO propagates at a speed of 5 days per phase from Phases 1 to 8 for 12 nonstop cycles. The middle 10 cycles are used to investigate what happens if the MJO is constantly propagating without decaying.

For all the Q_{MJO} experiments discussed above, similar to section 3.2, each set of experiments with an ensemble of 1,000 members has been performed. To simplify the Q_{MJO} pattern, constant RMM index amplitude is applied. Note that since we use amplitude greater than 1 as the threshold of strong MJO days, the averaged amplitude of each MJO event is greater than 1. Here we set the amplitude as 1.5 for all the idealized Q_{MJO} that is added into the idealized GCM. In all these experiments, Q_{MJO} starts at day 0 and the model is run for at least 60 days. The intensification and decaying processes of the MJO are ignored when constructing Q_{MJO} (see Text S3).

4.2. RMM Phases That Excite Large Extratropical Responses

From Figures 2f–2h, especially for Regions I and III, Phases 2 and 3 can induce strong positive response, while Phases 6 and 7 can induce strong opposite response. Here we investigate the PHASE(m)_15days experiments in which the MJO is in a constant RMM phase m for 15 days. Q_{MJO} is turned on at day 0 and turned off at day 15. The averaged extratropical response of days 28–32 is shown in Figure 6. The locations where large amplitude of extratropical response is generated by stationary heating (Figure 6) corresponds to where strong extratropical response is generated by *real* MJO heating (Figure 2e). This is consistent with what is shown in Goss and Feldstein (2018) that the spatial structure of MJO extratropical response does not depend on whether the heating is stationary or propagating. It is clear that Phase 2 and Phase 6 can induce the strongest response with opposite sign. This is consistent with Seo and Lee (2017). But this does not mean that the other phases are not important to the MJO extratropical response. Phases 1 and 3 (or 5 and 7) can also induce significant extratropical responses that are similar to Phase 2 or Phase 6, but with
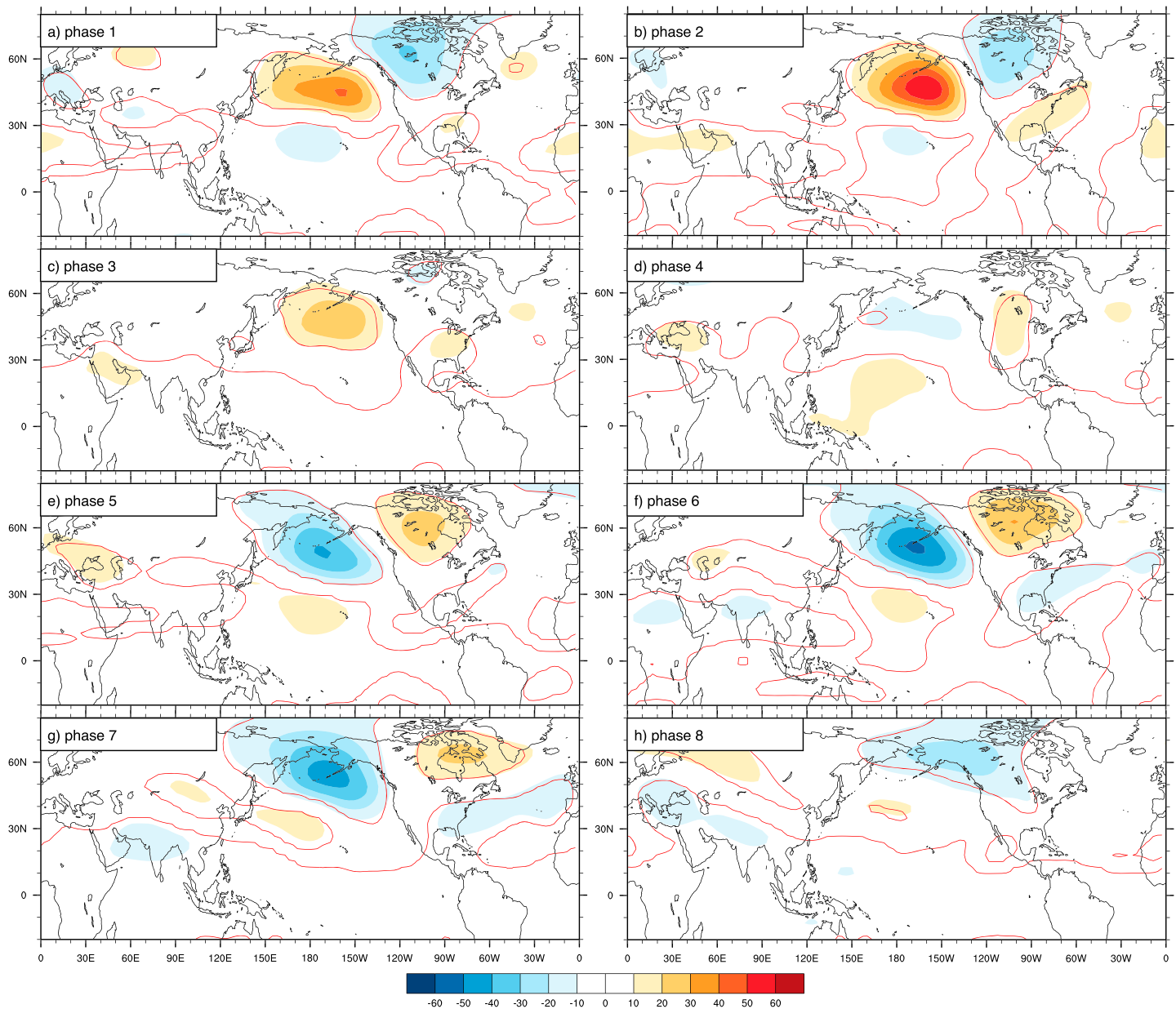
Figure 6. Averaged 300-hPa geopotential height anomalies between days 28 and 32 in the PHASE(m)_15days experiments (13−17 days after the external heating is switched off) for eight RMM phases. The red contours outline the regions where the height anomaly is statistically significant at the 95% level from the results of a Monte Carlo test (the same as Figures 1a−1e).

smaller amplitudes. These phases turn out to be also crucial for the timing, duration, and amplitude of the MJO extratropical response.

4.3. Extratropical Response to Different Idealized MJO Lifecycles

All sets of PHASE_s->e experiments have large response over central Pacific, Alaska and Western Canada, and eastern North America (see Figure S6). Therefore, we apply the same Regions I, II, and III as in Figure 2e in all the idealized heating experiments. We analyze the lag composites of each RMM phase from all sets of idealized MJO events experiments. For example, in Figure 7a, all the lag composites over Region I of PHASE_s->e experiments that Q_{MJO} goes through Phase 1 are included. The stationary heating experiments PHASE1_(n)days and the REAL_MJO experiment are also included. The lag composites of the other phases can be found in the rest of the Figure 7 or in Figure S7. The lag composites of Regions II and III are shown in
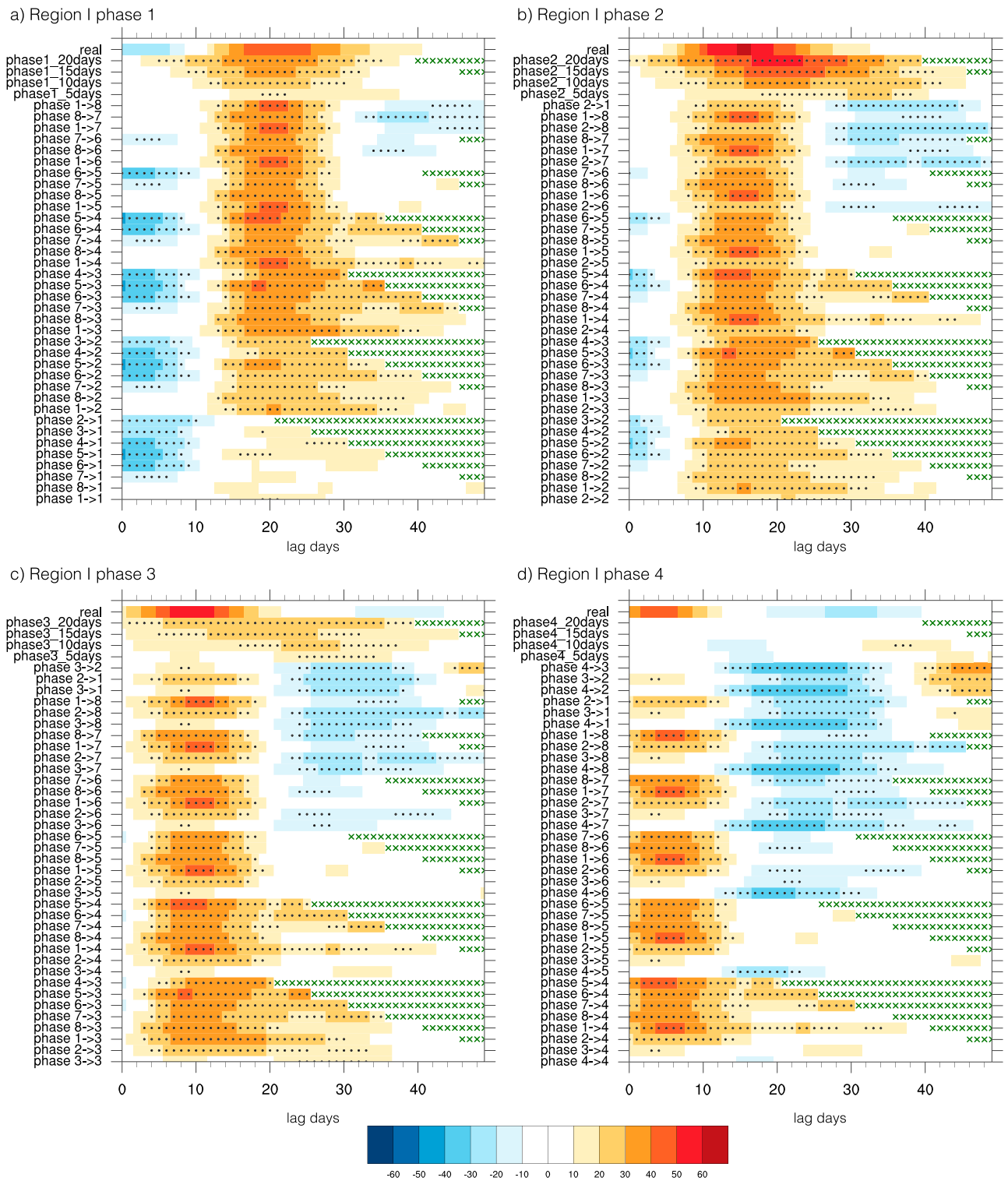
Figure 7. (a) Lag composites of 300-hPa geopotential height anomaly of RMM Phase 1 over Region I for PHASE_s->e, PHASE(m)_(n)days, and REAL_MJO (shown as *real* in the figure) experiments. Dotted days are statistically significant at the 95% level from the results of a Student's *t* test. The green crosses show the days that the experiment already ends on that day (as most of the experiments are only run for 60 days). Note that all the days with nonwhite color in the REAL_MJO row are statistically significant at the 95% level (see Figures 2f–2h). (b–d) The same as (a), but for RMM Phases 2–4, respectively.
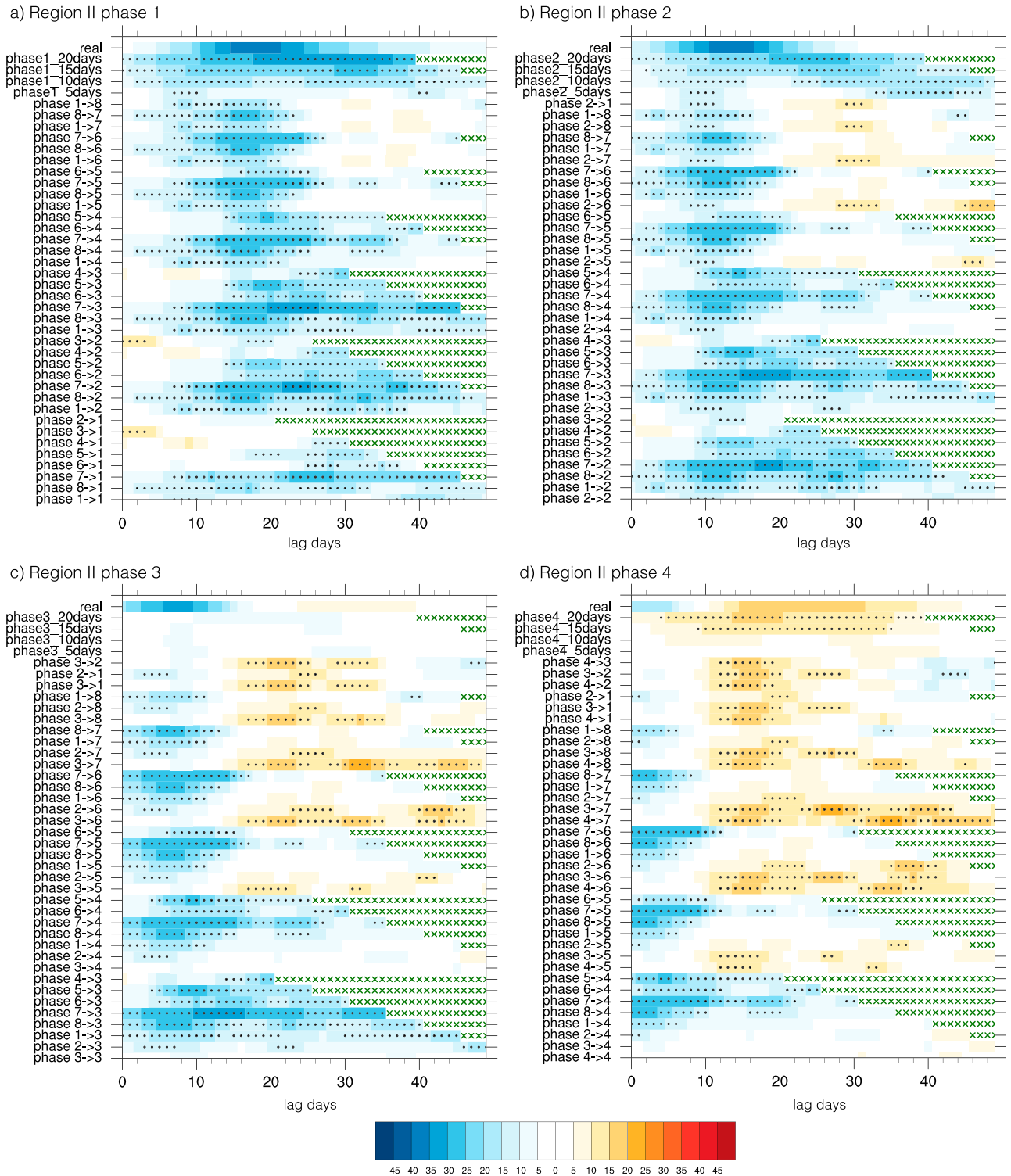
Figure 8. The same as Figure 7, but for Region II.

Figures 8 and S8 and 9 and S9, respectively. We will focus mostly on Phases 1–4 in our discussions (Phases 5–8 heating is exactly opposite to that of Phases 1–4 and gives rise to almost the same extratropical signal with opposite sign compared to Phases 1–4, and the conclusions for Phases 1–4 hold for Phases 5–8 except that the sign of the response is opposite).
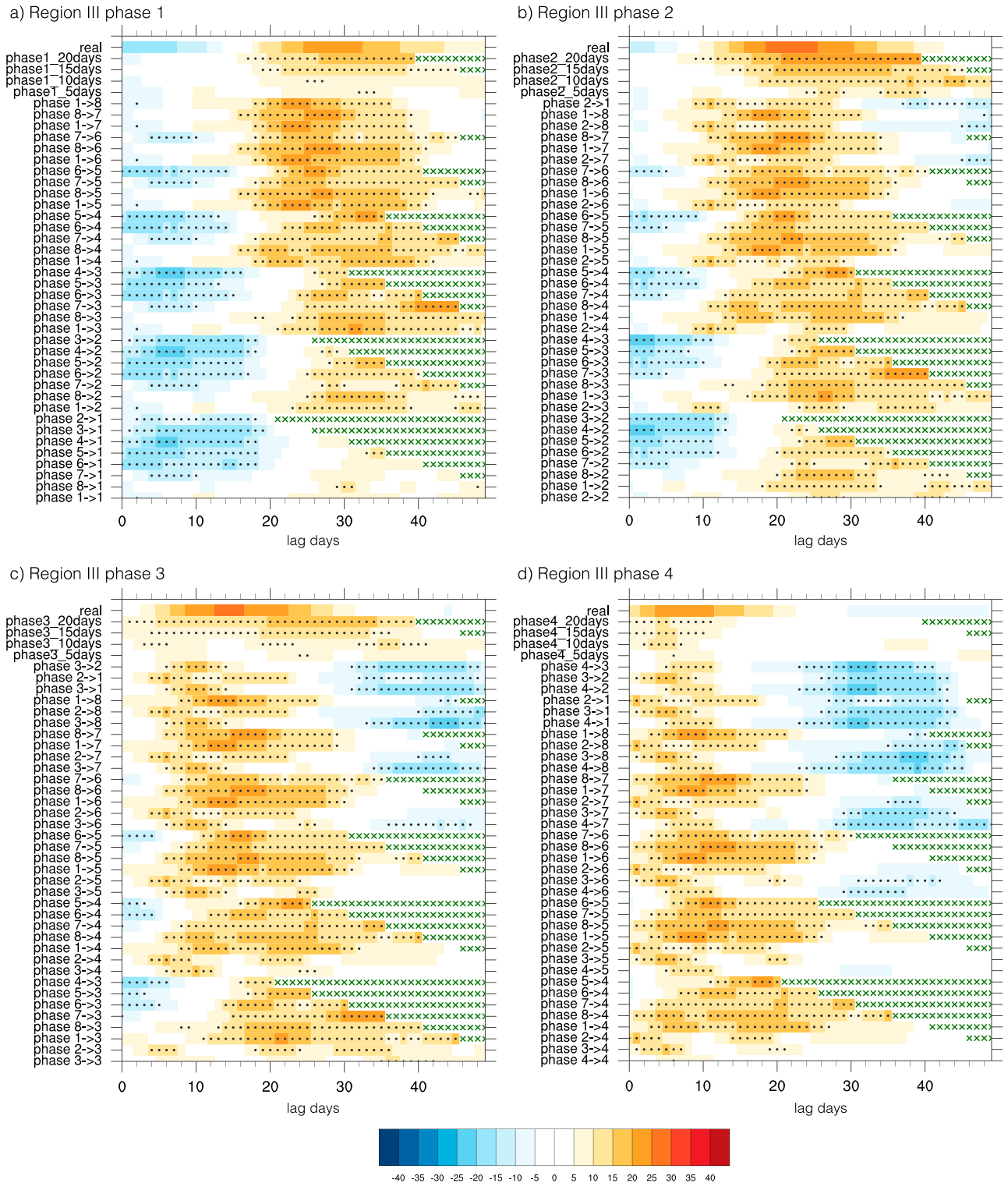
Figure 9. The same as Figure 7, but for Region III.

4.3.1. Comparing Realistic to Idealized MJO Heating

Overall, the REAL_MJO composites in Figures 7–9 are more or less consistent with the average over the PHASE_s->e experiments, with reasonable sign, timing, and amplitude. This is not surprising since the PHASE_s->e experiments contain most of the types of MJO events found in the REAL_MJO. However,

the evolution of the signal in the idealized MJO heating experiments displays large variations and individual idealized heating experiment often does not agree well with the REAL_MJO experiment. In most cases, the PHASE_s->e experiments do not produce the same signal as that of REAL_MJO.

In Figures 7a, 7c, 7d, 8c, 8d, 9a, 9b, and 9d, the sign of the response to REAL_MJO changes between early and later lag days. For individual PHASE_s->e experiments, not all of the MJO events have both strong positive and negative signals, and the amplitude has large variations among individual idealized heating events. In the early lags before the sign changes, for Regions I and III of Phase 1 (Figures 7a and 9a), the signal from REAL_MJO clearly comes from the events that have been initiated earlier than Phase 7. This signal is not directly related to Phase 1 heating as the signal cannot be induced by the stationary heating experiments (second to fifth rows in each panel). The subsequent positive signal for REAL_MJO in Phase 1 comes more from the events that propagate into Phase 3, while the MJO events that decay before Phase 3 have a weaker signal.

Therefore, the signal of REAL_MJO can only be regarded as the on-average MJO extratropical response. The characteristics of the signal of each MJO event depend on the specifics of the MJO event, for example, initiation and decay phase, and can be quite different from the mean signal (REAL_MJO or composites from Reanalysis). Thus, the mean signal may not be a useful tool to predict the extratropical response of a specific MJO event. In the real world, the spatial structure of the heating can be significantly different for individual MJO events, even if the RMM index is in the same phase. This may lead to further inconsistency between the extratropical response of a specific MJO event and the mean response.

4.3.2. The Phases That Induce Strong Signals

The strongest extratropical response is found when the MJO goes through specific series of RMM phases. Though Phases 2 and 6 induce the strongest extratropical response if the heating is stationary, the strongest signals are not only associated with these two phases.

For Region I, strong positive signal is found at lag days 10 to 30 after Phase 1 in Figure 7a. If Q_{MJO} ends at Phase 1 or Phase 2, the amplitude of the extratropical response is weaker than that of the MJO events that propagate into Phase 3. But the amplitude does not become stronger if the MJO continue to propagate after Phase 3. The amplitude of the extratropical response for the MJO events that ends in Phases 4–7 is nearly the same as those that ends in Phase 3. Therefore, in order to excite a strong response in Region I, the MJO has to propagate into Phase 3.

Figure S10 is the same as Figures 7 and S7, but the order of the y axis is rearranged so that adjacent rows have the same initiation phase. We can focus on lag composites of Phase 3 as we already know that only when the MJO propagates into Phase 3, the response in Region I will be strong. Clearly, if the MJO is initiated at Phase 2 or Phase 3, the response is weaker than that for MJO initiated at Phase 1 or earlier. Therefore, one can conclude that though Phase 2 is the favorable phase to excite a strong extratropical response, the MJO also needs to be initiated at least in Phase 1 and at least propagates into Phase 3 to generate strong response in Region I. Similarly, for the opposite signal, the MJO needs to be initiated at least in Phase 5 and at least propagates into Phase 7.

Similar feature can also be found in Region III. From Figure 9a, to excite strong MJO response in Region III, the MJO has to propagate into Phase 4 or Phase 5; from Figure S12c, the MJO needs to be initiated before (or at) Phase 1 to make the response stronger.

As Phases 1 and 3 can also induce significant extratropical responses that is similar to Phase 2 (see section 4.2), the signal of Phases 1 and 3 will help intensify the pattern induced by Phase 2. This makes the extratropical responses stronger when the MJO propagates through a series of phases (1–3 and 5–7 for the opposite signal) compared to when the MJO is only strong in Phase 2 or Phase 6 since a consistent excitation of a similar Rossby wave is maintained over a longer duration.

4.3.3. Duration of MJO Response

The duration of the response is also sensitive to the start and end phases of the MJO. In Figure 7c, the lag composite after Phase 3 shows that the positive height response that is in between lag day 0 and lag day 20 can extend to day 30 if the MJO decays before Phase 4 or Phase 5. However, if the MJO propagates into Phase 5 or Phase 6, the positive anomaly disappears after day 20 and the sign of the anomaly shifts to negative. Similar feature can be found for Region II (Figure 8c) and Region III (Figure 9c). As shown in section 4.2, Phases 5 and 6 excite the opposite extratropical response to Phase 2; when the MJO

propagates into Phases 5 and 6, negative signal will be generated to destructively interfere with the original positive signal excited by the previous phases (Phases 1–3), eventually reversing the sign of the response. However, if the MJO decays at Phase 3 or Phase 4, no opposite signal will be generated by the MJO to destructively interfere with the original response, and the original positive (or negative) signal will just slowly decay. Thus, the response can be long lasting if the MJO decays in Phase 3 or Phase 4. Similarly, the signal excited by Phases 5 to 7 can also be long lasting if the MJO decays in Phase 7 or Phase 8.

4.3.4. Timing of MJO Response

As discussed above, if positive anomaly induced by the MJO already exists in one extratropical region, once the MJO propagates into phases that generate the opposite signal, the opposite signal needs to first weaken the original positive anomaly and then changes the signal of the anomaly. Hence, if the original positive signal is stronger, it would take longer time for the opposite signal to compensate for the original one, which will delay the timing of the opposite signal. As shown earlier in this section (4.3.4), the strength of the original signal depends on in which phase the MJO is initiated (the MJO needs to be initiated before Phase 2 or Phase 6 to generate stronger responses). Such dependence of the timing on the initiation phase can be clearly seen in the response in Region III. In lag composite of Phase 1 (Figure S12a), if we take the negative signal before lag day 20 as the original signal, and the positive signal as the opposite signal, the original signal is stronger if the MJO is initiated in Phase 5 or Phase 4. The opposite signal, which is in positive sign, appears later if the original signal is stronger than that in the cases the original signal is weaker (MJO initiated in Phase 8 or Phase 7).

In summary, the timing, duration, and amplitude of the MJO extratropical response not only depend on whether the MJO goes through the most favorable phase to excite strong extratropical response (Phases 2 and 6) but also strongly depend on which phase the MJO is initiated in and during which phase the MJO decays.

4.4. Slow (Long Lifetime) Idealized MJO Heating

The results from PHASE_s->e with a slower MJO propagation speed (also longer lifetime) of 8 days per phase instead of 5 days per phase are shown in Figures 10 and 11. The conclusions discussed in section 4.3 hold the following: (1) Individual experiment frequently does not resemble the composite signal, consistent with section 4.3.1. For example, in Region III after Phase 1 (Figure 11a), the composite REAL_MJO signal changes from negative to positive of about the same amplitude, while in individual experiments those that show strong positive signals at early lags generally show weak negative signals at later lag and vice versa. (2) The signal of Region I is strongest (Figures 10a and 10c) when the MJO propagates through Phases 1 to 3, which is consistent with section 4.3.2. (3) The duration of the signal, or whether the signal changes sign, depends on whether the MJO decays before a specific phase or propagates into later phases (Figures 10b, 11b, and 11d), which is consistent with section 4.3.3. These features also exist for the opposite signal related to Phases 5–7.

The main difference between the response of 8 and 5 days per phase is that the amplitude of the response in 8 days per phase is stronger. This is reasonable as the MJO stays longer in the phases that can induce strong extratropical responses (Phases 1–3 and 5–7); the response accumulates and will become stronger in these slow-propagating (also long-lasting) MJO events. Again, this is consistent with Yadav and Straus (2017). The timing of the maximum signal is delayed in Phases 1 and 5 for Regions I and III (Figures 7a, S7e, 9a, S9e, 10a, S16e, 11a, and S18e), especially for Region III. As Phases 1–3 and 5–7 are the phases required to excite a stronger signal, as the MJO events with the propagation speed of 8 days per phase stay longer in these phases, it is reasonable that the timing of the maximum signal is delayed.

4.5. Cyclic MJO

The limit of MJO without initiation or decaying is the CYCLIC_MJO experiment. As discussed previously, no long-lasting signal would exist if the MJO is constantly propagating, since opposite signal would be generated by the following RMM phases, which can destroy the original signal. The duration of the signal in the CYCLIC_MJO (Figure 12) is shorter than REAL_MJO (e.g., the duration of positive signal in Region I Phase 3 is about 20 days in REAL_MJO and 15 days in CYCLIC_MJO). In addition, in the CYCLIC_MJO experiments, though Phases 1–3 can excite strong extratropical response, in all cases in these experiments, the response of Phases 1–3 needs to first compensate for the residual response from Phases 5–7, which will
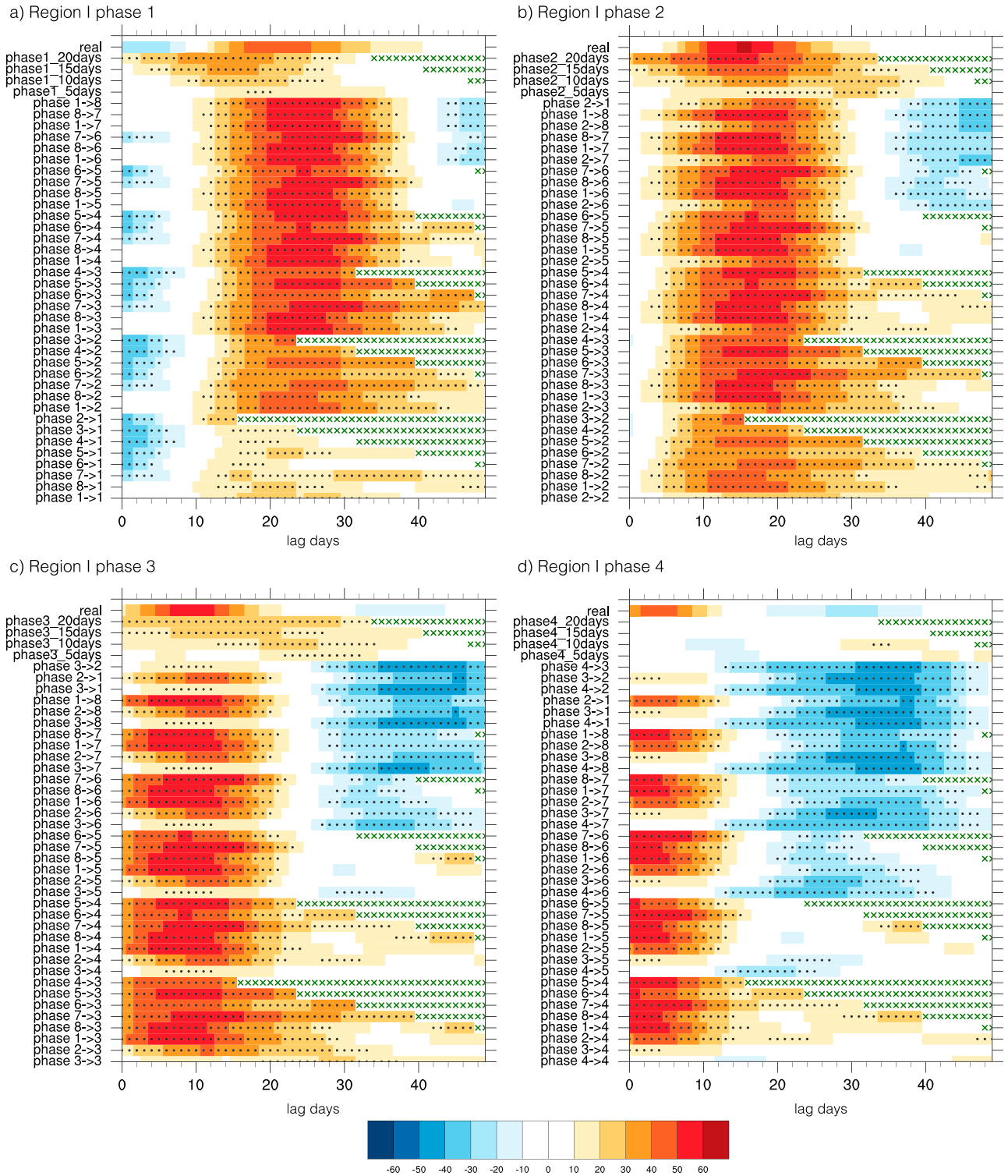
Figure 10. The same as Figure 7, but for PHASE_s->e experiments with an MJO propagation speed of 8 days per phase instead of 5 days per phase.

weaken the amplitude that can be reached generated by Phases 1–3. Therefore, the signal in the CYCLIC_MJO experiments is much weaker than that in REAL_MJO and weaker than most of the cases in PHASE_s->e experiments. This further confirms that the initiation and decaying of the MJO is crucial to excite a strong and long-lasting MJO extratropical response.
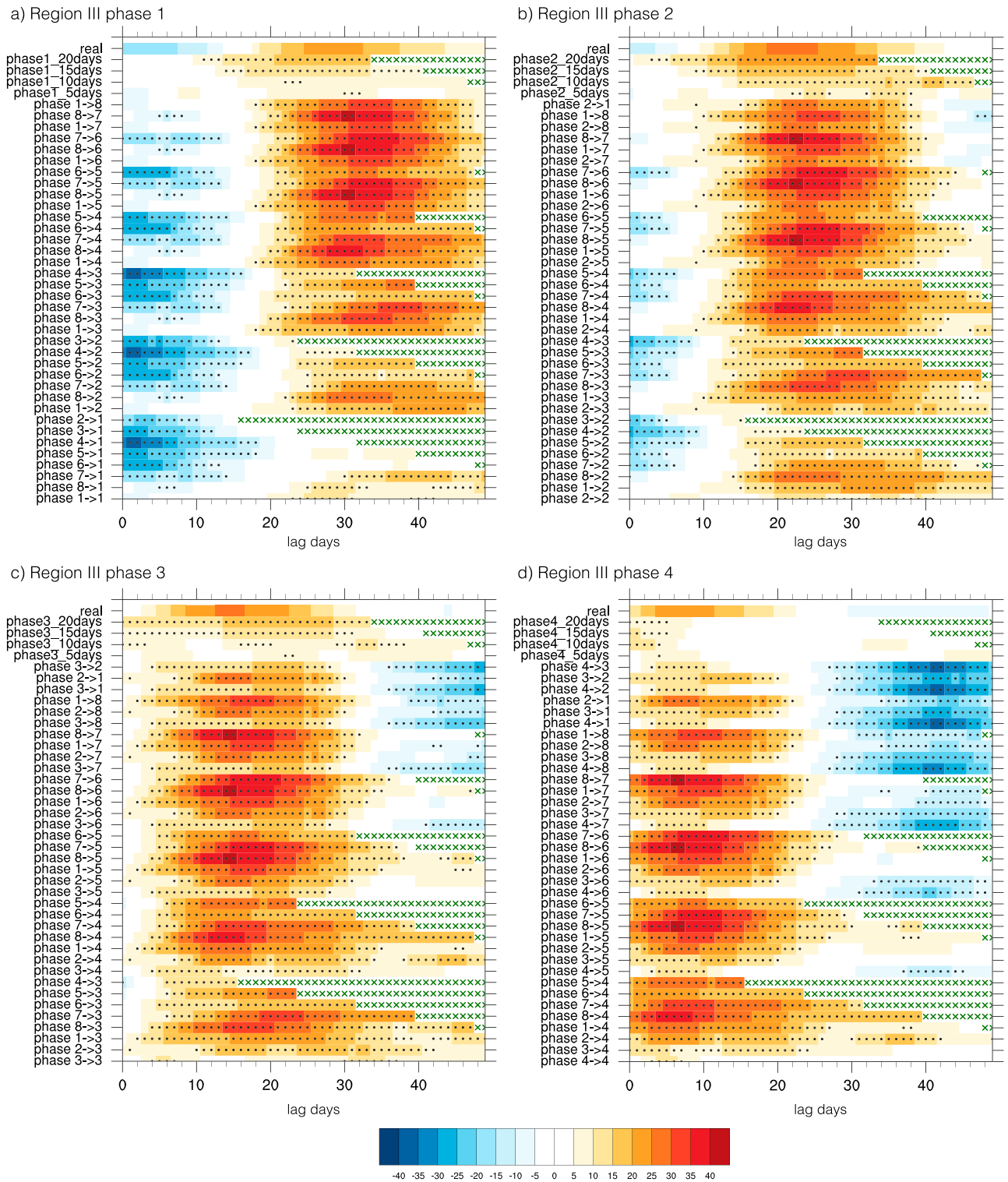
Figure 11. The same as Figure 10, but for Region III.

4.6. The Role of MJO Intensity

PHASE_s->e experiments have also been performed with the intensity of the MJO doubled (RMM index amplitude equals to 3.0). The results of the three regions are shown in Figures S22–S24. As one would
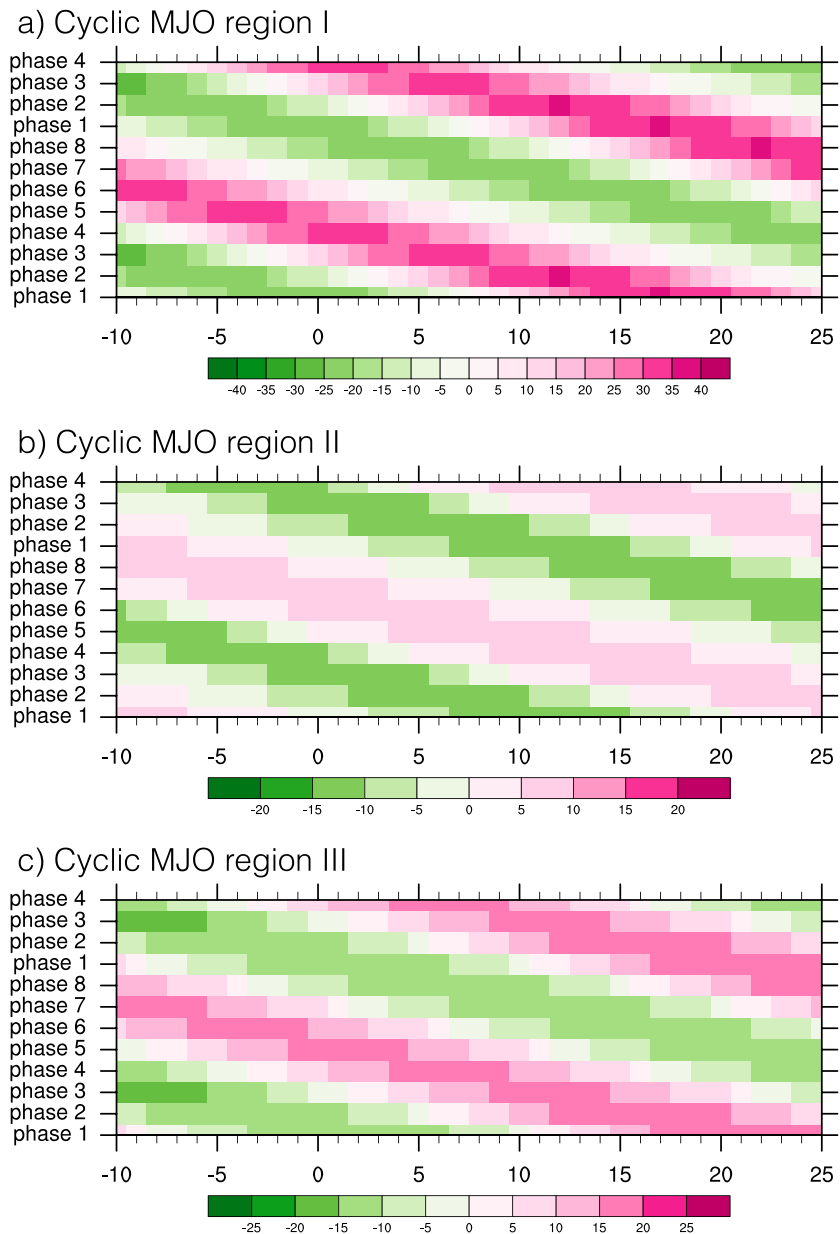
Figure 12. The same as Figures 2f–2h, but for CYCLIC_MJO experiments.

expect, stronger MJO will give rise to stronger Rossby wave source; the extratropical response becomes stronger than the normal MJO amplitude (RMM index amplitude equals to 1.5) experiment. However, the timing and duration of the response is almost the same as that from the normal MJO amplitude experiment, though the double-intensity MJO experiment is less noisy. So if the intensity of the MJO is constant during the MJO events, how strong the intensity is does not seem to significantly modify the temporal evolution of the MJO extratropical response.

5. Stationary Wave Model Experiments

Most of the experiments mentioned above have been repeated with the stationary wave model. The results of PHASE_s->e experiments are shown in Figures 13 and S25–S27. The stationary wave model yields rather similar results compared to those from the full idealized model. Despite stronger
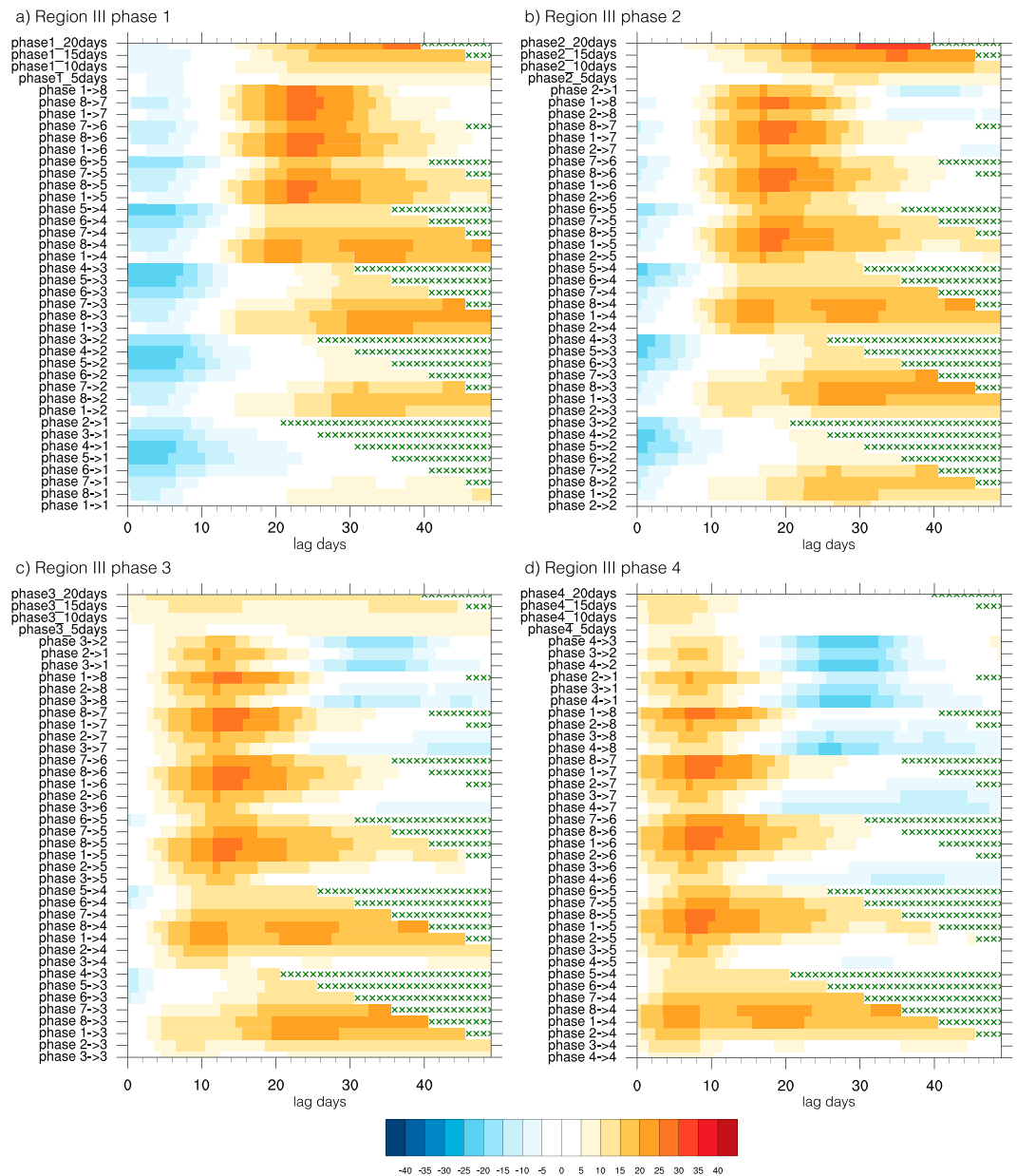
Figure 13. The same as Figure 8, but for results from the stationary wave model. The statistical significance levels are not shown since there is only one run in each experiment in the stationary wave model.

damping used in the stationary wave model, the amplitude of the signal is still slightly larger than those in the idealized GCM, suggesting that the transient eddies in the idealized GCM probably mainly act to damp the response induced by the MJO. In Figure 13, the response in Region III has been shown, which has very similar timing, duration, and amplitude as that shown in Figure 9 (negative signal in lag days after Phases 3 and 4 appears earlier in the stationary wave model) but is much less noisy. Though the stationary wave model is a more simplified version of the model, nonlinearity is preserved in the model, which may potentially be important for the evolution of the MJO extratropical response. As it is much cheaper to run the stationary wave model (only one run is required compared to about 1,000 runs required for the full idealized GCM to obtain large signal-to-noise ratio) and the results are similar to the full idealized model, the stationary wave model can be a useful tool to study the MJO extratropical response.

6. Summary and Discussions

It is shown by previous studies that the MJO can excite Rossby waves, which propagate into the extratropics and modify midlatitude circulation. As the circulation is modified, midlatitude surface weather, for example, surface air temperature, extratropical cyclone activity, and precipitation, will be modulated by the MJO. By analyzing Reanalysis data, we found that three regions, one over central North Pacific, one over Alaska and western Canada, and one over eastern North America, highlight the propagation of the Rossby wave. These three regions can be used to represent the Rossby wave over the Pacific and North America induced by the MJO.

Our idealized GCM, in which we put MJO-induced heating as an external forcing, can capture the MJO extratropical response reasonably well. A large number of ensembles (1,000) have been performed with the idealized GCM. The results show that if the sample size in the idealized model is the same as that in the Reanalysis, the MJO extratropical response does not seem to be robust. About 10 ensemble members with the same sample size are required to reach a robust result. As the lag composites from the Reanalysis are still much noisier than the ensemble mean of the idealized GCM ensemble, we suggest that the extratropical response derived from the Reanalysis data set may still be not robust.

Experiments with different MJO propagation speed (also different lifetime) show that slow-propagating MJO excites stronger extratropical response than fast-propagating MJO, which is consistent with Yadav and Straus (2017). RMM Phases 2 and 6 have been found to excite the strongest extratropical response with opposite sign among the RMM phases, which is consistent with Seo and Lee (2017). Phases 1 and 3 can excite similar extratropical signal as Phase 2 with smaller amplitude, and Phases 5 and 7 can excite similar extratropical signal as Phase 6 with smaller amplitude. These phases also play important roles to induce strong and long-lasting MJO extratropical response.

Idealized MJO events are added into the idealized model to study the role of propagation and lifetime on modulating the MJO extratropical response. The experiments are performed with MJO of different propagation speed (5 and 8 days per phase) and different lifetime (the number of phases MJO lasts). The signal of individual MJO event can be very different from the mean MJO signal. The strongest signal can be induced when the MJO propagates through a series of RMM phases (usually 1–3 and 5–7). The duration of the MJO response, or whether the signal shifts sign, depends on if the MJO quickly decays (around Phases 4 and 8) after going through the series of phases to induce the strong response or if the MJO still propagates into later phases (into Phase 5/6 or 1/2). The timing of the signal is early if the MJO is initiated close to the series of RMM phases, which can induce strong signal (initiated in Phase 8/1 or 4/5), but the timing will be delayed if the MJO is initiated much earlier. The timing, duration, and amplitude of the MJO extratropical response strongly depend on the initiation and decaying of the MJO. The slow-propagating (also long lifetime) idealized MJO events induce stronger extratropical response, and the timing of the response is slightly different than the faster-propagating events. The cyclic MJO heating (nonstop propagating MJO without decaying) generates much weaker extratropical response, and the duration of the response is much shorter. In addition, the stationary wave model, which is much easier to run computationally, yields very similar results as the large ensemble of the original idealized model. Thus, the stationary wave model can be a useful tool to study the MJO extratropical response.

As MJO extratropical response can last more than 30 days if the MJO decays at specific phases (Phases 4/5 and 8/1), there is potential for extended range forecasts in the extratropics for these MJO events. In addition, as the sign and duration of the extratropical response strongly depend on whether the MJO can propagate through Phase 4/5 (8/1), whether the MJO propagates through these phases is crucial to the forecast of MJO extratropical impact in subseasonal timescale. Also, as the MJO needs to propagate through Phases 1–3 or 5–7 to excite the strongest response, whether the MJO can propagate across Phase 3 or Phase 7 is important in the prediction of the amplitude of MJO extratropical response.

Our results suggest that MJO events with specific lifecycles can excite substantially different extratropical responses compared to lag composites that only consider the number of days after a RMM phase, which represent averaging over many different types of events. Hence, it is not surprising that statistical forecasts based only on the initial RMM phase (e.g., Johnson et al., 2014) are not skillful at week 4. Since it takes about 7–10 days for the extratropical response to develop (Goss & Feldstein, 2018; also see Figure 7 second row two

to fifth row in each panel), the MJO extratropical response on week 4 depends on whether the MJO decays or still propagates during weeks 2 and 3. To improve the forecast for week 4, one needs to be able to predict the state of the MJO in weeks 2 and 3. However, the challenge is that not only do we need a good forecast of the MJO in weeks 2 and 3, we also need to know the MJO extratropical response for the different MJO evolution, which we currently do not have sufficient samples to determine accurately from Reanalysis data.

Nevertheless, our results do confirm the potential for dynamical models to predict the MJO-related extratropical signals several weeks in advanced, given that the evolution of the MJO is predictable out to 3–4 weeks in advance, and the MJO-excited wave train can last several weeks after the MJO decays. On the other hand, other factors such as errors or variations in the structure of the heating and the background flow may also strongly impact the evolution of the MJO-excited Rossby wave train. These factors will be explored in future studies.

References

Adames, Á. F., Patoux, J., & Foster, R. C. (2014). The contribution of extratropical waves to the MJO wind field. *Journal of the Atmospheric Sciences*, *71*(1), 155–176. https://doi.org/10.1175/JAS-D-13-084.1

Baxter, S., Weaver, S., Gottschalck, J., & Xue, Y. (2014). Pentad evolution of wintertime impacts of the Madden–Julian Oscillation over the contiguous United States. *Journal of Climate*, *27*(19), 7356–7367. https://doi.org/10.1175/JCLI-D-14-00105.1

Becker, E. J., Berbery, E. H., & Higgins, R. W. (2011). Modulation of cold-season U.S. daily precipitation by the Madden–Julian Oscillation. *Journal of Climate*, *24*(19), 5157–5166. https://doi.org/10.1175/2011JCLI4018.1

Cassou, C. (2008). Intraseasonal interaction between the Madden–Julian Oscillation and the North Atlantic Oscillation. *Nature*, *455*(7212), 523–527. https://doi.org/10.1038/nature07286

Chang, E. K. (2006). An idealized nonlinear model of the Northern Hemisphere winter storm tracks. *Journal of the Atmospheric Sciences*, *63*(7), 1818–1839. https://doi.org/10.1175/JAS3726.1

Chang, E. K. (2009). Diabatic and orographic forcing of northern winter stationary waves and storm tracks. *Journal of Climate*, *22*(3), 670–688. https://doi.org/10.1175/2008JCLI2403.1

Dee, D. P., Uppala, S. M., Simmons, A. J., Berrisford, P., Poli, P., Kobayashi, S., et al. (2011). The ERA-Interim reanalysis: Configuration and performance of the data assimilation system. *Quarterly Journal of the Royal Meteorological Society*, *137*(656), 553–597. https://doi.org/10.1002/qj.828

Deng, Y., & Jiang, T. (2011). Intraseasonal modulation of the North Pacific storm track by tropical convection in boreal winter. *Journal of Climate*, *24*(4), 1122–1137. https://doi.org/10.1175/2010JCLI3676.1

Donald, A., Meinke, H., Power, B., de Maia, A. H. N., Wheeler, M. C., White, N., et al. (2006). Near-global impact of the Madden-Julian Oscillation on rainfall. *Geophysical Research Letters*, *33*, L09704. https://doi.org/10.1029/2005GL025155

Flatau, M., & Kim, Y. (2013). Interaction between the MJO and polar circulations. *Journal of Climate*, *26*(11), 3562–3574. https://doi.org/10.1175/JCLI-D-11-00508.1

Garfinkel, C. I., Feldstein, S. B., Waugh, D. W., Yoo, C., & Lee, S. (2012). Observed connection between stratospheric sudden warmings and the Madden–Julian Oscillation. *Geophysical Research Letters*, *39*, L18807. https://doi.org/10.1029/2012GL053144

Goss, M., & Feldstein, S. B. (2015). The impact of the initial flow on the extratropical response to Madden–Julian Oscillation convective heating. *Monthly Weather Review*, *143*(4), 1104–1121. https://doi.org/10.1175/MWR-D-14-00141.1

Goss, M., & Feldstein, S. B. (2017). Why do similar patterns of tropical convection yield extratropical circulation anomalies of opposite sign? *Journal of the Atmospheric Sciences*, *74*(2), 487–511. https://doi.org/10.1175/JAS-D-16-0067.1

Goss, M., & Feldstein, S. B. (2018). Testing the sensitivity of the extratropical response to the location, amplitude, and propagation speed of tropical convection. *Journal of the Atmospheric Sciences*, *75*(2), 639–655. https://doi.org/10.1175/JAS-D-17-0132.1

Grise, K. M., Son, S., & Gyakum, J. R. (2013). Intraseasonal and interannual variability in North American storm tracks and its relationship to equatorial Pacific variability. *Monthly Weather Review*, *141*(10), 3610–3625. https://doi.org/10.1175/MWR-D-12-00322.1

Guo, Y., Shinoda, T., Lin, J., & Chang, E. K. (2017). Variations of Northern Hemisphere storm track and extratropical cyclone activity associated with the Madden–Julian Oscillation. *Journal of Climate*, *30*(13), 4799–4818. https://doi.org/10.1175/JCLI-D-16-0513.1

Held, I. M., & Suarez, M. J. (1994). A proposal for the intercomparison of the dynamical cores of Atmospheric General Circulation Models. *Bulletin of the American Meteorological Society*, *75*(10), 1825–1830. https://doi.org/10.1175/1520-0477(1994)075<1825:APFTIO>2.0.CO;2

Held, I. M., Ting, M., & Wang, H. (2002). Northern winter stationary waves: Theory and modeling. *Journal of Climate*, *15*(16), 2125–2144. https://doi.org/10.1175/1520-0442(2002)015<2125:NWSWTA>2.0.CO;2

Henderson, S. A., Maloney, E. D., & Barnes, E. A. (2016). The influence of the Madden–Julian Oscillation on Northern Hemisphere winter blocking. *Journal of Climate*, *29*(12), 4597–4616. https://doi.org/10.1175/JCLI-D-15-0502.1

Henderson, S. A., Maloney, E. D., & Son, S. (2017). Madden–Julian Oscillation Pacific teleconnections: The impact of the basic state and MJO representation in general circulation models. *Journal of Climate*, *30*(12), 4567–4587. https://doi.org/10.1175/JCLI-D-16-0789.1

Hoskins, B. J., & Karoly, D. J. (1981). The steady linear response of a spherical atmosphere to thermal and orographic forcing. *Journal of the Atmospheric Sciences*, *38*(6), 1179–1196. https://doi.org/10.1175/1520-0469(1981)038<1179:TSLROA>2.0.CO;2

Jin, F., & Hoskins, B. J. (1995). The direct response to tropical heating in a baroclinic atmosphere. *Journal of the Atmospheric Sciences*, *52*(3), 307–319. https://doi.org/10.1175/1520-0469(1995)052<0307:TDRTTH>2.0.CO;2

Johnson, N. C., Collins, D. C., Feldstein, S. B., L'Heureux, M. L., & Riddle, E. E. (2014). Skillful wintertime North American temperature forecasts out to 4 weeks based on the state of ENSO and the MJO. *Weather and Forecasting*, *29*(1), 23–38. https://doi.org/10.1175/WAF-D-13-00102.1

Kiladis, G. N., Dias, J., Straub, K. H., Wheeler, M. C., Tulich, S. N., Kikuchi, K., et al. (2014). A comparison of OLR and circulation-based indices for tracking the MJO. *Monthly Weather Review*, *142*(5), 1697–1715. https://doi.org/10.1175/MWR-D-13-00301.1

Kim, H. M., Webster, P. J., Toma, V. E., & Kim, D. (2014). Predictability and prediction skill of the MJO in two operational forecasting systems. *Journal of Climate*, *27*(14), 5364–5378. https://doi.org/10.1175/JCLI-D-13-00480.1

Klingaman, N. P., Woolnough, S. J., Jiang, X., Waliser, D., Xavier, P. K., Petch, J., et al. (2015). Vertical structure and physical processes of the Madden-Julian Oscillation: Linking hindcast fidelity to simulated diabatic heating and moistening. *Journal of Geophysical Research: Oceans*, *120*, 4690–4717. https://doi.org/10.1002/2014JD022374

Kunkel, K. E., Easterling, D. R., Kristovich, D. A., Gleason, B., Stoecker, L., & Smith, R. (2012). Meteorological causes of the secular variations in observed extreme precipitation events for the conterminous United States. *Journal of Hydrometeorology*, *13*(3), 1131–1141. https://doi.org/10.1175/JHM-D-11-0108.1

L'Heureux, M. L., & Higgins, R. W. (2008). Boreal winter links between the Madden–Julian Oscillation and the Arctic Oscillation. *Journal of Climate*, *21*(12), 3040–3050. https://doi.org/10.1175/2007JCLI1955.1

Lee, Y.-Y., & Lim, G.-H. (2012). Dependency of the North Pacific winter storm tracks on the zonal distribution of MJO convection. *Journal of Geophysical Research*, *117*(A1), D14101. https://doi.org/10.1029/2011JA017246

Liebmann, B., & Smith, C. A. (1996). Description of a complete (interpolated) outgoing longwave radiation dataset. *Bulletin of the American Meteorological Society*, *77*, 1275–1277.

Lim, Y., Son, S., & Kim, D. (2018). MJO prediction skill of the subseasonal-to-seasonal prediction models. *Journal of Climate*, *31*(10), 4075–4094. https://doi.org/10.1175/JCLI-D-17-0545.1

Lin, H., & Brunet, G. (2009). The influence of the Madden–Julian Oscillation on Canadian wintertime surface air temperature. *Monthly Weather Review*, *137*(7), 2250–2262. https://doi.org/10.1175/2009MWR2831.1

Lin, H., & Brunet, G. (2011). Impact of the North Atlantic Oscillation on the forecast skill of the Madden-Julian Oscillation. *Geophysical Research Letters*, *38*, L02802. https://doi.org/10.1029/2010GL046131

Lin, H., Brunet, G., & Derome, J. (2009). An observed connection between the North Atlantic Oscillation and the Madden–Julian Oscillation. *Journal of Climate*, *22*(2), 364–380. https://doi.org/10.1175/2008JCLI2515.1

Lin, H., Brunet, G., & Mo, R. (2010). Impact of the Madden–Julian Oscillation on wintertime precipitation in Canada. *Monthly Weather Review*, *138*(10), 3822–3839. https://doi.org/10.1175/2010MWR3363.1

Ma, C., & Chang, E. K. (2017). Impacts of storm-track variations on wintertime extreme weather events over the continental United States. *Journal of Climate*, *30*(12), 4601–4624. https://doi.org/10.1175/JCLI-D-16-0560.1

MacRitchie, K., & Roundy, P. E. (2016). The two-way relationship between the Madden–Julian Oscillation and anticyclonic wave breaking. *Quarterly Journal of the Royal Meteorological Society*, *142*(698), 2159–2167. https://doi.org/10.1002/qj.2809

Madden, R. A., & Julian, P. R. (1971). Detection of a 40–50 day oscillation in the zonal wind in the tropical Pacific. *Journal of the Atmospheric Sciences*, *28*(5), 702–708. https://doi.org/10.1175/1520-0469(1971)028<0702:DOADOI>2.0.CO;2

Madden, R. A., & Julian, P. R. (1972). Description of global-scale circulation cells in the tropics with a 40–50 day period. *Journal of the Atmospheric Sciences*, *29*(6), 1109–1123. https://doi.org/10.1175/1520-0469(1972)029<1109:DOGSCC>2.0.CO;2

Madden, R. A., & Julian, P. R. (1994). Observations of the 40–50-day tropical oscillation—A review. *Monthly Weather Review*, *122*(5), 814–837. https://doi.org/10.1175/1520-0493(1994)122<0814:OOTDTO>2.0.CO;2

Matthews, A. J. (2008). Primary and successive events in the Madden–Julian Oscillation. *Quarterly Journal of the Royal Meteorological Society*, *134*(631), 439–453. https://doi.org/10.1002/qj.224

Matthews, A. J., Hoskins, B. J., & Masutani, M. (2004). The global response to tropical heating in the Madden–Julian Oscillation during the northern winter. *Quarterly Journal of the Royal Meteorological Society*, *130*(601), 1991–2011. https://doi.org/10.1256/qj.02.123

Moore, R. W., Martius, O., & Spengler, T. (2010). The modulation of the subtropical and extratropical atmosphere in the Pacific Basin in response to the Madden–Julian Oscillation. *Monthly Weather Review*, *138*(7), 2761–2779. https://doi.org/10.1175/2010MWR3194.1

Mori, M., & Watanabe, M. (2008). The growth and triggering mechanisms of the PNA: A MJO-PNA coherence. *Journal of the Meteorological Society of Japan*, *86*(1), 213–236. https://doi.org/10.2151/jmsj.86.213

O'Gorman, P. A. (2011). The effective static stability experienced by eddies in a moist atmosphere. *Journal of the Atmospheric Sciences*, *68*(1), 75–90. https://doi.org/10.1175/2010JAS3537.1

Oliver, E. C., & Thompson, K. R. (2012). A reconstruction of Madden–Julian Oscillation variability from 1905 to 2008. *Journal of Climate*, *25*(6), 1996–2019. https://doi.org/10.1175/JCLI-D-11-00154.1

Pfahl, S., Schwierz, C., Croci-Maspoli, M., Grams, C. M., & Wernli, H. (2015). Importance of latent heat release in ascending air streams for atmospheric blocking. *Nature Geoscience*, *8*(8), 610–614. https://doi.org/10.1038/ngeo2487

Ray, P., & Li, T. (2013). Relative roles of circumnavigating waves and extratropics on the MJO and its relationship with the mean state. *Journal of the Atmospheric Sciences*, *70*(3), 876–893. https://doi.org/10.1175/JAS-D-12-0153.1

Ray, P., Zhang, C., Dudhia, J., & Chen, S. S. (2009). A numerical case study on the initiation of the Madden–Julian Oscillation. *Journal of the Atmospheric Sciences*, *66*(2), 310–331. https://doi.org/10.1175/2008JAS2701.1

Riddle, E. E., Stoner, M. B., & Johnson, N. C. (2013). The impact of the MJO on clusters of wintertime circulation anomalies over the North American region. *Climate Dynamics*, *40*(7-8), 1749–1766. https://doi.org/10.1007/s00382-012-1493-y

Sardeshmukh, P. D., & Hoskins, B. J. (1988). The generation of global rotational flow by steady idealized tropical divergence. *Journal of the Atmospheric Sciences*, *45*(7), 1228–1251. https://doi.org/10.1175/1520-0469(1988)045<1228:TGOGRF>2.0.CO;2

Schreck, C. J., Cordeira, J. M., & Margolin, D. (2013). Which MJO events affect North American temperatures? *Monthly Weather Review*, *141*(11), 3840–3850. https://doi.org/10.1175/MWR-D-13-00118.1

Seo, K., & Lee, H. (2017). Mechanisms for a PNA-like teleconnection pattern in response to the MJO. *Journal of the Atmospheric Sciences*, *74*(6), 1767–1781. https://doi.org/10.1175/JAS-D-16-0343.1

Seo, K., & Son, S. (2012). The global atmospheric circulation response to tropical diabatic heating associated with the Madden–Julian Oscillation during northern winter. *Journal of the Atmospheric Sciences*, *69*(1), 79–96. https://doi.org/10.1175/2011JAS3686.1

Straub, K. H. (2013). MJO initiation in the real-time multivariate MJO index. *Journal of Climate*, *26*(4), 1130–1151. https://doi.org/10.1175/JCLI-D-12-00074.1

Tseng, K.-C., Barnes, E. A., & Maloney, E. D. (2018). Prediction of the midlatitude response to strong Madden-Julian Oscillation events on S2S time scales. *Geophysical Research Letters*, *45*(1), 463–470. https://doi.org/10.1002/2017GL075734

Vecchi, G. A., & Bond, N. A. (2004). The Madden–Julian Oscillation (MJO) and northern high latitude wintertime surface air temperatures. *Geophysical Research Letters*, *31*, L04104. https://doi.org/10.1029/2003GL018645

Vitart, F. (2017). Madden-Julian Oscillation prediction and teleconnections in the S2S database. *Quarterly Journal of the Royal Meteorological Society*, *143*(706), 2210–2220. https://doi.org/10.1002/qj.3079

Vitart, F., & Jung, T. (2010). Impact of the Northern Hemisphere extratropics on the skill in predicting the Madden–Julian Oscillation. *Geophysical Research Letters*, *37*, L23805. https://doi.org/10.1029/2010GL045465

Wang, H., & Ting, M. (1999). Seasonal cycle of the climatological stationary waves in the NCEP–NCAR Reanalysis. *Journal of the Atmospheric Sciences*, *56*(22), 3892–3919. https://doi.org/10.1175/1520-0469(1999)056<3892:SCOTCS>2.0.CO;2

Wheeler, M. C., & Hendon, H. H. (2004). An all-season real-time multivariate MJO index: Development of an index for monitoring and prediction. *Monthly Weather Review*, *132*(8), 1917–1932. https://doi.org/10.1175/1520-0493(2004)132<1917:AARMMI>2.0.CO;2

Xia, X., & Chang, E. K. (2014). Diabatic damping of zonal index variations. *Journal of the Atmospheric Sciences*, *71*(8), 3090–3105. https://doi.org/10.1175/JAS-D-13-0292.1

Xiang, B., Zhao, M., Jiang, X., Lin, S., Li, T., Fu, X., & Vecchi, G. (2015). The 3–4-week MJO prediction skill in a GFDL coupled model. *Journal of Climate*, *28*(13), 5351–5364. https://doi.org/10.1175/JCLI-D-15-0102.1

Yadav, P., & Straus, D. M. (2017). Circulation response to fast and slow MJO episodes. *Monthly Weather Review*, *145*(5), 1577–1596. https://doi.org/10.1175/MWR-D-16-0352.1

Yang, X., & Chang, E. K. (2006). Variability of the Southern Hemisphere winter split flow—A case of two-way reinforcement between mean flow and eddy anomalies. *Journal of the Atmospheric Sciences*, *63*(2), 634–650. https://doi.org/10.1175/JAS3643.1

Yoo, C., Feldstein, S., & Lee, S. (2011). The impact of the Madden-Julian Oscillation trend on the Arctic amplification of surface air temperature during the 1979–2008 boreal winter. *Geophysical Research Letters*, *38*, L24804. https://doi.org/10.1029/2011GL049881

Zhang, C., & Dong, M. (2004). Seasonality in the Madden–Julian Oscillation. *Journal of Climate*, *17*(16), 3169–3180. https://doi.org/10.1175/1520-0442(2004)017<3169:SITMO>2.0.CO;2

Zhao, C., Li, T., & Zhou, T. (2013). Precursor signals and processes associated with MJO initiation over the tropical Indian Ocean. *Journal of Climate*, *26*(1), 291–307. https://doi.org/10.1175/JCLI-D-12-00113.1

Zheng, C., Chang, E. K. M., Kim, H., Zhang, M., & Wang, W. (2018). Impacts of the Madden–Julian Oscillation on storm-track activity, surface air temperature, and precipitation over North America. *Journal of Climate*, *31*(15), 6113–6134. https://doi.org/10.1175/JCLI-D-17-0534.1

Zhou, S., L'Heureux, M., Weaver, S., & Kumar, A. (2012). A composite study of the MJO influence on the surface air temperature and precipitation over the continental United States. *Climate Dynamics*, *38*(7-8), 1459–1471. https://doi.org/10.1007/s00382-011-1001-9

Zhou, S., & Miller, A. J. (2005). The interaction of the Madden–Julian Oscillation and the Arctic Oscillation. *Journal of Climate*, *18*(1), 143–159. https://doi.org/10.1175/JCLI3251.1